Parameter Dependent Rates in Transition State Theory for Periodically Driven Systems

Bachelor thesis of
Melissa Jacqueline Lober

August 26, 2018

Supervisor: Prof. Dr. Jörg Main

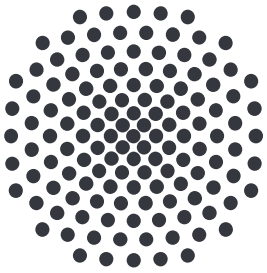

1. Institut für Theoretische Physik
Universität Stuttgart
Pfaffenwaldring 57, 70550 Stuttgart

Contents

1 Introduction

It is known from simple middle school chemistry that reactants react into products during a chemical reaction. Such a transition is only possible, when the energy of the reactant configuration exceeds a certain threshold, which, in chemistry, is known as the activation energy. Fig. 1.1 illustrates a simplified chemical reaction in which a ball, as a simple example for a reactant, has to overcome a barrier of a certain height in order to reach the other side of this barrier and become a product. As soon as the reactant's total energy exceeds the barrier's energy, it is able to transition into a product. In this simple one-dimensional example the maximum of the barrier, i.e. the saddle, clearly separates reactants from products, meaning if the ball passes the maximum of the barrier, it will fall down to the product side. When the separation of reactants and products is known, it is possible to propagate reactants along the reaction coordinate and estimate the flux of reactants transitioning into products. The calculation of reaction rates and reaction pathways is the central topic of the Transition State Theory (TST) [1–18].

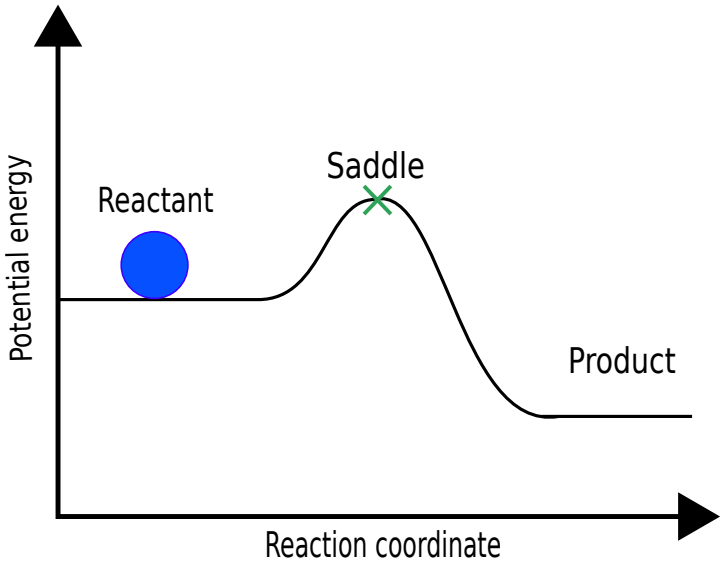

Figure 1.1: Simplified illustration of a chemical reaction along the reaction coordinate in which a ball (reactant) has to overcome the energy of the saddle in order to become a product.

A real chemical reaction usually holds many degrees of freedom. Therefore it is a great challenge in TST to accurately describe a higher-dimensional system with one direction "over the saddle" (the reaction coordinate) and many other degrees of freedom (the bath coordinates). When a chemical reaction is pertubated, i.e. driven by a time-dependent external force, the potential energy surface of the system will become time-dependent itself. In reality, such an external force could be the result of a time-dependent electric field, for example. The separation of reactant and product configurations, which enables the calculation of reaction rates, is much more complex when the system is high-dimensional and time-dependent. Previous research of the ITP1 in this field [19–21] has led to the separation of phase space of periodically driven systems through a time-dependent hypersurface, the Dividing Surface (DS) [19, 20]. This research has recently laid the foundation for the computation of reaction rates which are determined by the flux of reactants through this dividing surface.

Building on the previous research of the ITP1, this work deals with the task of calculating rate constants for a numerical simulation of reactants crossing the DS in a two-dimensional time-dependent system. These rate constants depend on multiple aspects of the system such as the concrete properties of the external driving as well as the composition of the propagated ensemble of reactants. The central task of this work is to determine in what manner the rate constant depends on the specific structure and movement of the potential energy surface. For this purpose, the work aims at the development of an ensemble that leads to a rate constant that is a reflection of the system's dynamics, as well as the development of a uniform procedure that can be used to estimate these rate constants.

Outline of the thesis

The structure of this work is the following. Chapter 2 provides a brief overview on how reaction rates are defined and estimated, how the DS is calculated in a one-dimensional as well as in a higher-dimensional and time-dependent system using neural networks and lastly it introduces the properties of the system that will be simulated in this work.

Chapter 3 introduces several aspects of the system that impact the reaction rate (in a sometimes undesired way) and what can be done to estimate a rate that is as accurate and also as comparable to the rates of other systems as possible.

Chapter 4 starts off with the task of generating an ensemble whose reaction rate does not depend on its position on the potential energy surface along the reaction coordinate. Once this ensemble is found, several investigations are performed to estimate its optimal mean energy in order to obtain reaction rates that mainly reflect the system's dynamics and are not a sole property of the ensemble itself. Further, the dependence of the

rate constant on the phase of movement of the system is determined as well as the rate's behavior for an increasing number of reactants within the ensemble. Lastly, the dependence of the rate constant on the structure of the potential energy landscape is examined.

Chapter 5 introduces an additional ensemble that is generated to increase the number of the so-called "critical particles" whose reaction rate reflects the dynamic's of the system close to the barrier. With this ensemble, several investigations of the previous chapter are repeated and compared: the dependence of the rate constant on the phase of movement of the system; the rate's behavior for an increasing number of reactants within the ensemble and the dependence of the rate constant on the structure of the potential energy landscape.

2 Theory

2.1 Computing Rate Constants

The reaction rate of a chemical reaction describes how fast particles react from one side of the barrier to the other side. In order to estimate this reaction rate, it is necessary to track the decrease of the number of reactants over time $N_\mathrm{r}(t)$ during the simulation. The number of reactants decreases by one for each reaction from reactant to product. It is crucial that particles only react once, since it would otherwise lead to an overestimation of the reaction rate. It is stated in [22] that for a chemical reaction, the number of reactions decays exponentially with

$$N_\mathrm{r}(t) - N_\mathrm{r}(\infty) = N_{\mathrm{r},0} \exp(-k\,t)\,, \tag{2.1}$$

where k denotes the rate constant, $N_\mathrm{r}(\infty)$ is the number of reactants that do not perform a reaction and $N_{\mathrm{r},0}$ is the total number of reactants that react during the simulation. If the rate constant k has a positive value, the number of reactants decays exponentially in time. Exemplary, an exponential decay of the number of reactants over time due to

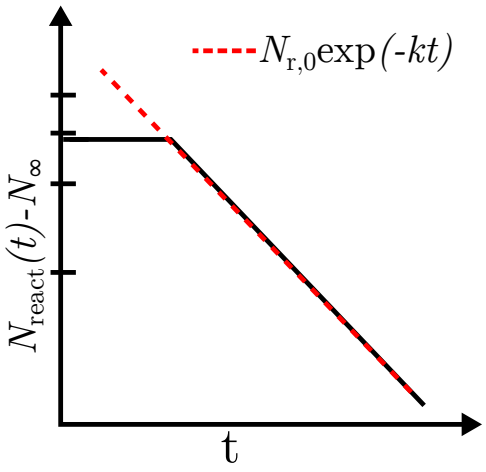

Figure 2.1: Example of an exponential decay of reactive particles over time with a logarithmic scale, fitted with an exponential function that leads to the rate constant k.

the reactions of $N_{\mathrm{r},0}$ particles is displayed in Fig. 2.1 with a logarithmic scaled y-axis. The decay is not expected to start right after the start of the propagation, since the propagated particles need a certain amount of time to reach the barrier. This causes the curve in Fig. 2.1 to remain constant for a certain transisiton time in the beginning of the propagation. As soon as the exponential decay starts, the curve is fitted with a function equal to Eq. (2.1) leading to the reaction constant k.

As mentioned above, the rate constant can only be estimated if the number of reactants is known over time. The number of reactants decreases with each particle crossing the DS. To know if and at what time a reaction has happened, it has to be determined whether a particle is a reactant or a product for each time step of the simulation. This can only be done when the point of transition from a reactant configuration to a product configuration is clearly defined. The next section will deal with the task of determining this point of transition.

2.2 Obtaining the Dividing Surface

This section will give a short outline of all the steps that are taken to obtain the DS in a one-dimensional system, as well as in a multidimensional time-dependent system.

In a static, one-dimensional Hamiltonian system, the point of transition from a reactant configuration to a product configuration is given by the maximum of the barrier in the potential energy landscape. Fig. 2.2 displays a separation of phase space by two manifolds one of which is the stable manifold $\mathcal{W}_{\mathrm{s}}$ and one the unstable manifold $\mathcal{W}_{\mathrm{u}}$. Theoretically, particles that are initialized on a point of the stable manifold reach the maximum of the saddle exponentially fast and stay on the saddle for an infinite amount of time. Particles initialized on the unstable manifold show the same behavior when propagated in backward time. The stable and the unstable manifold intersect at a single point, called the "Normally Hyperbolic Invariant Manifold" (NHIM). Further information on the concept of a NHIM can be found in Refs. [23–25]. Its position x_{NHIM} marks the separation between reactants and products for all v_x. In Fig. 2.2, this separation of phase space is displayed as a dividing line (DL). Whether a propagated particle is a reactant or a product can be determined by comparing its position along the reaction coordinate x_{p} to the position x_{DL} of the dividing line:

$$\begin{aligned} x_{\mathrm{p}} < x_{\mathrm{DL}} &\rightarrow \text{particle is a reactant} \quad , \\ x_{\mathrm{p}} > x_{\mathrm{DL}} &\rightarrow \text{particle is a product} \quad . \end{aligned}$$

All particles are initialized in one of the four areas separated by the manifolds in Fig. 2.2. Area I and III are non-reactive, meaning that particles that are initialized in one of the two areas remain to be reactants or products respectively throughout the propagation.

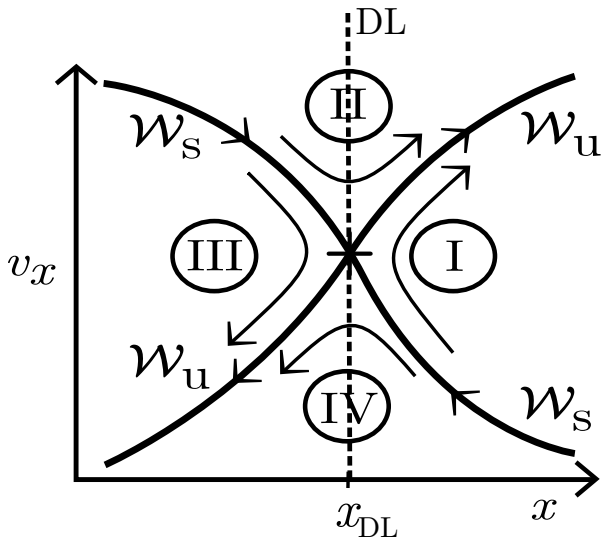

Figure 2.2: Phase space of a one-dimensional static system. $\mathcal{W}_\mathrm{s}$ denotes the stable, $\mathcal{W}_\mathrm{u}$ the unstable manifold. The cross marks the intersection of these manifolds. The phase space is separated into the four areas I-IV. The dividing line DL separates the phase space into a reactant ($x < x_\mathrm{DL}$) and a product configuration ($x > x_\mathrm{DL}$).

Areas II and IV are reactive areas in phase space. All of the particles initialized in area II will eventually transition from a reactant into a product, when being propagated for an infinite amount of time. The same applies for area IV for propagation in backward time.

For a time-dependent system, the DL is time-dependent as well. When the saddle performs an oscillation, so does the DL. However, in a time-dependent system, the manifolds do not necessarily intersect at the maximum of the saddle. The movement of a time-dependent DL is detached from the movement of the saddle which is complicating its calculation. In a one-dimensional system, the position of a time dependent DL is given by the transition state (TS) trajectory [26–35] which describes the trajectory of a particle that is bound to the saddle region for all time.

When dealing with a multidimensional time-dependent system, the distinction between reactants and products is more complex than in the one-dimensional system above. In a system with n degrees of freedom, there is one reaction coordinate x and $n-1$ bath coordinates that are determined by the structure of the potential energy surface of the system. The reaction coordinate denotes the unstable direction of the barrier, since the barrier oscillates along x. The phase space has the dimension $2n$, e.g. position and the respective velocity. In order to divide a $2n$-dimensional phase space into a reactant and a product configuration, the dividing line of the 1D-system extends to a $(2n-1)$-

dimensional hypersurface, the so-called "dividing surface" (DS) [19, 20]. Particles may only cross the DS once, since it would otherwise lead to an overestimation of the reaction rate. Therefore, the DS must be recrossing-free. However, if the system has closed reactant or product basins, the particles might be reflected globally at the boundaries of the system which could cause them to react infinite times [36–43]. The global recrossing-free property of the DS is given by open basins of the system.

This DS is attached to the NHIM which is again the $(2n-2)$-dimensional intersection of the $(2n-1)$-dimensional manifolds. For a better visualizaton of the system, the reaction coordinate can be seen as perpendicular to the NHIM, while the bath coordinates can be seen as parallel to it. Given a set of bath coordinates and a certain time t, the position (x, v_x) of the NHIM can be calculated by using for example the Lagrangian Descriptor (LD) [19, 44, 45]. An application of the LD-method in the calculation of the TS-trajectory can be found in [43, 46]. The DS is obtained by extending the NHIM for all possible values of v_x.

The LD-method is one possible way to calculate points on the DS. However, it is stated in Ref. [21] that this method is quite complex and time-consuming. In this paper it was shown that using the so-called "Binary-contraction-method" (BC) is a more efficient method for the task of computing positions on the NHIM. Without the propagation of particles, it is unknown if and where their trajectories will intersect with the DS. Therefore, the position of the DS would have to be computed for every trajectory individually, which is very time-consuming for a propagation of several millions of particles. An efficient possibility to represent the DS of a moving saddle is was found in [20]. Hence, several positions of the DS are calculated with the BC-method and then interpolated using an artificial neural network to obtain a well-defined and continuous DS. The following section will introduce neural networks and how they can be used to interpolate data.

2.3 Neural Networks

A neural net is inspired by the biological nerve networks of a brain. Just like the human brain, neural networks learn how to solve problems by comparing them to similar problems whose solutions are already known. For example, a neural network can learn to identify human-written digits when provided with a high number of examples that were already pre-assigned with the respective digit.

Here, neural networks are used to obtain a continuous time-dependent dividing surface. The previous section already explaines how to compute single positions of the NHIM out of a given set of bath coordinates and how to obtain the respective dividing surface. Given the pre-calculated positions for a known set of bath coordinates, the neural net

is able to learn how to reconstruct these positions as well as how to approximate the positions for further bath coordinates. Such an interpolation of the NHIM's positions is necessary to obtain a well-defined DS that clearly separates particles with arbitrary trajectories into reactants and products. Neural networks are well suited for this task, since the input data (here: bath coordinates and time) does not need to be ordered or have a specific dimension. In addition, neural networks have the ability to smooth and correct points that differ a lot from the rest of the data.

The following subsections present the general structure of a neural network, as well as the process of training a neural net for a given set of data.

Structure of a Neural Network

A neural network usually consists out of several layers that each contain several neurons. The connection of two neurons of neighboring layers transmits an information from one neuron to the next, just like a synapse in the human brain. Before dealing with the network as a whole, its most basic component, the neuron, is presented.

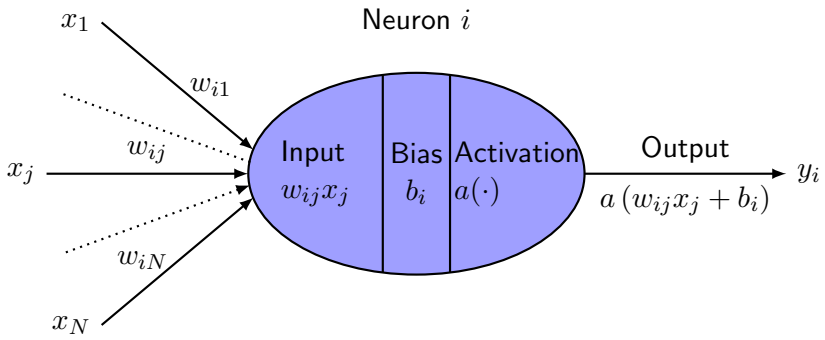

Figure 2.3: Schematic illustration of a neuron, obtained from [47]. The inputs x_i are weighted with w_{ij} and the neuron calculates the output y_i for a given bias b and activation function a.

A neuron alters and transmits information. It has at least one input value and exactly one output value. Each input has a so-called "weight" w_i that determines the importance of its value to the output of the neuron. Figure 2.3 illustrates the structure of a single neuron i in a layer l. The bias b determines the likelyhood of a neuron to output large values for the given weighted inputs. When the weightend sum $\sum_{i=1}^{N} w_i\, x_i$ over N inputs exceeds this bias, the neuron is more likely to output a value that is large and therefore of greater importance for the calculation of the neurons in the next layer. To avoid linear mapping between the input and the output values, the output value is calculated using an activation function. The output value y_i of the neuron is calculated using the equation [47]

$$y_i = a\left(\sum_{i=1}^{N} w_{ij} \cdot x_j\right) + b_i \quad . \tag{2.2}$$

In early models of neural networks, the neuron's output was binary (0 or 1) according to whether the weighted sum $\sum_{i=1}^{N} w_i\, x_i$ over N inputs exceeded a given threshold value or not. Such a neuron is called "perceptron" and corresponds to a neuron with a Heaviside function as the activation function. In the past, networks of perceptrons did not have a broad area of application, since they do not have the desired ability to learn autonomously. A learning algorithm alters specific parameters in order to correct a wrong output. The network can correct such a wrong output when a slight variation of the weights or biases leads to a slight change of the output value. Since a perceptron can only produce output values of 0 or 1, a network of perceptrons is suitable for mimicing boolean structures but not so much for correcting its own output values. By modifying a neuron with an activation function that is a smoothed out version of the Heaviside function, it can have input as well as output values within a whole range of values determined by a. In general, this activation function is nonlinear. Such a function can be the reverse tangent, for example.

When solving more complex problems, it is usually necessary to introduce so-called "hidden layers" of neurons. Figure 2.4 shows the structure of a network with a number of k hidden layers that has a similar structure to the one used in this work. There are three input neurons that have a constant output value. There is one output neuron that provides the final result of the net. All the neurons inbetween the input and the output neurons are part of a hidden layer. Each output of a neuron in a previous layer is an input of all the neurons in the following layer. Such networks are called "feedforward" neural networks, since there are no loops in the network and the output of a neuron is always fed forward. For example, the input neurons provide the values of y, v_y and t for which the position of the DS shall be calculated. Given these parameters, the output neuron then provides the position x of the NHIM at which the DS is attached.

Training a Neural Network

The neural network is trained with a set of training-data that contains the pre-calculated output values for a given set of input values. A cost function

$$C(y, \tilde{y}) = \frac{1}{2n} \sum_{i=1}^{n} |y_i - \tilde{y}(x_i)|^2 \tag{2.3}$$

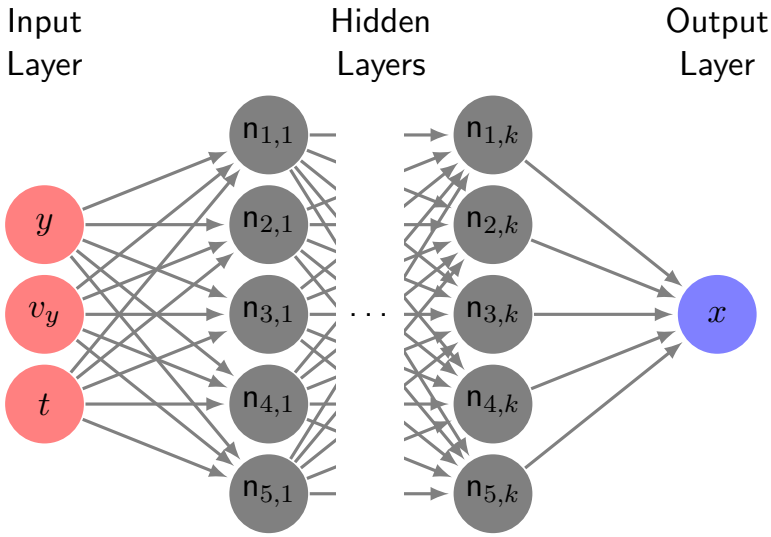

Figure 2.4: Schematic illustration of a neural network with k hidden layers. The input layer constists of three neurons with the constant input values y, v_y, t. The hidden layers each contain several neurons. The output layer constists out of one neuron with the output value x.

is introduced that determines the deviation of the training data y to the outputs $\tilde{y}$ of the neural net for the same input values x_i. The number of training points is given by n.

To achieve the highest possible accuracy, the cost function must be minimized, so that the prediction of the neural net is as close to the training data as possible. As mentioned above, the network is able to learn and correct its output values by changing the weight and bias-parameters. According to Ref. [20], this can be done using the gradient descent method which repeatedly computes the gradient of the cost function as a function of the weight and bias parameters and changes these parameters in a way that leads to a decrease of the cost function until a minimum is found. Every layer and each bias and weight lead to a different gradient. For the determiniation of all gradients, a back-propagation algorithm is used. To speed up the procedure of computing the overall gradient of the cost function, the training data is split into smaller batches of randomly selected training data. By averaging over the gradients of the small batches, the overall gradient can be estimated satisfactorily. Such an approach is referred to as a *stochastic* gradient descent method. In a so-called "epoche" the complete set of training data is used once to calculate the cost function's gradient.

Accuracy of the Dividing Surface

Beside the cost function that describes the deviation between the neural network's output and the data it is trained with, there is another cost function that determines the deviation between the net's output and additional data that is not used for training but for the validation of the network. A low validation cost indicates that points other than the training data are well approximated by the network. However, if the training cost is decreasing over several epoches while the validation cost remains constant, the network is likely to have overfitted the training data, meaning the training data is approximated with a very high accuracy while other points do not match the desired output. In an ideal case, the training cost as well as the validation cost decrease monotonously until the last training epoche is completed, so that the whole DS is approximated as well as possible.

Another measurement of the accuracy of the DS is the number of re-crossing particles that occur when an ensemble is propagated. Since the DS ought to clearly separate possible reactants from products, the occurance of a re-crossing particle indicates a false or inaccurate approximation of the DS.

2.4 System

2.4.1 Model Potential with a Driven Rank-1 Saddle

The potential energy surface of the system is modeled by a driven rank-1 saddle potential by

$$V(x,y,t) = E_\mathrm{b}\,\exp\left(-a\,\left[x-\hat{x}\sin(\omega_x\,(t-t_0))\right]^2\right) + \frac{\omega_y^2}{2}\,\left(y-\frac{2}{\pi}\,\hat{y}\,\arctan(\tilde{a}\,x)\right)^2 \quad . \tag{2.4}$$

Along the reaction coordinate x, the potential performs a periodic oscillation with the angular frequency ω_x and the amplitude $\hat{x}$. The parameter E_b determines the height of a Gaussian shaped energy barrier in x-direction with the width a. The so-called "barrier-phase" t_0 denotes a time shift of its oscillation. The second term of the potential is time-independent and describes the potential in y-direction. This term is harmonic along the bath coordinate y and is coupled non-linearly to the reaction coordinate x. As it can be seen in Figure 2.5, the two minima of the potential are shifted in y-direction. The parameter $\hat{y}$ determines the minima's maximum deviation from $y = 0.0$. The parameters ω_y and $\tilde{a}$ are further parameters to tune the potential.

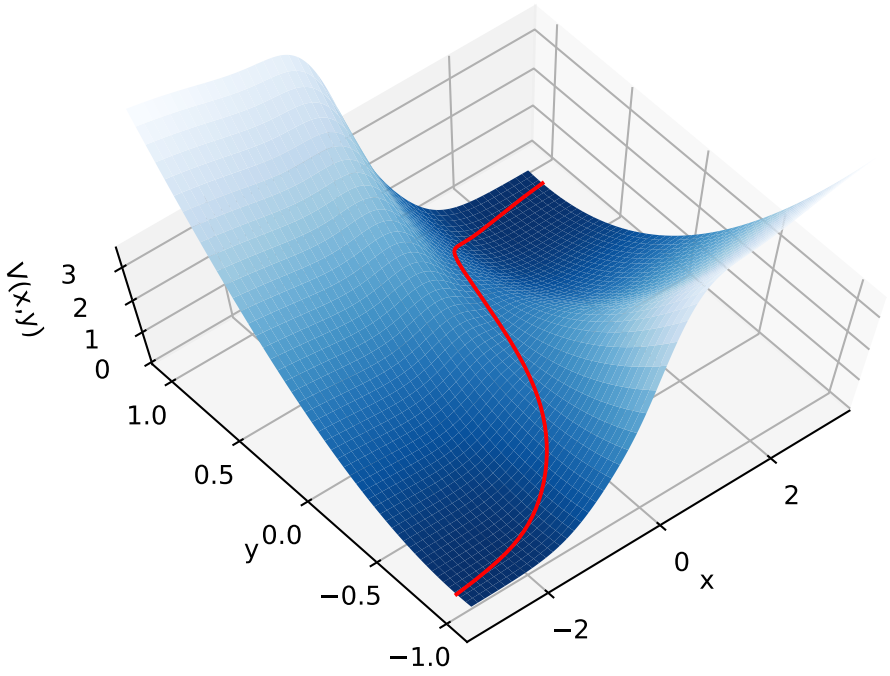

Figure 2.5: Potential defined in Eq. (2.4) for the standard parameters. Darker shades of blue indicate a low value of the potential whereas bright shades of blue represent a high value. The red line across the potential's barrier marks the minimum-energy-path (MEP).

In a later section, the path of minimum energy over the potential's barrier will gain importance. In Figure 2.5 it is displayed as a red line across the barrier. It can be calculated by derivating the potential's minimum with respect to y. The following equation defines this so-called *minimum-energy-path*, short MEP,

$$\begin{aligned}
&\frac{\partial}{\partial y} V(x,y,t) = 0 \\
&\Leftrightarrow \frac{\partial}{\partial y}[E_\mathrm{b} \exp(-a\,(x - \hat{x}\sin(\omega_x\,(t-t_0))^2) + \frac{\omega_y}{2}(y - \frac{2}{\pi}\,\hat{y}\,\arctan(\tilde{a}\,x))^2] = 0 \\
&\Leftrightarrow y = \frac{2}{\pi}\,\hat{y}\,\arctan(\tilde{a}\,x) \quad . \qquad (2.5)
\end{aligned}$$

The standard setting for the potential's parameters used in this work is

$$\begin{aligned} E_\mathrm{b} = 2.0\,; \qquad a = 1.0\,; \qquad \hat{x} = 0.4\,; \qquad \omega_x = \pi\,; \\ t_0 = 0.0\,; \qquad \omega_y = 1.0\,; \qquad \hat{y} = 1.0\,; \qquad \tilde{a} = 2.0\,, \end{aligned} \tag{2.6}$$

if no different parameters are given. Throughout this work, the parameters t_0, E_b, ω_x, $\hat{x}$ and $\hat{y}$ will be varied.

2.4.2 Ensemble

The particles propagated in this work are part of a canonical ensemble. The ensemble is defined through the following properties: the total number N of particles in it; the range $(x \pm \Delta, y \pm \Delta)$ that restricts the particles' positions; the value of the Boltzmann's constant $k_\mathrm{B}T$; as well as the potential's values $V(x, y, t_0)$ at the positions of the particles (x, y) and a barrier-phase of t_0.

The ensemble's total energy is the sum of kinetic and potential energy and follows a Chi-squared distribution. The ensemble is generated using a seeded pseudo random number generator.

For the special case that the ensemble is positioned at a single point on the potential, the potential energy does not impact the energy distribution within the ensemble by more than an offset value. For a potential of zero, the probability $f(E_\mathrm{tot})$ for an occupied energy state E_tot is reduced to the Maxwell-Boltzmann-distribution

$$f(E_\mathrm{tot}) = v \exp\left(-\frac{\frac{m}{2}\,v^2}{k_\mathrm{B}T}\right) \quad , \tag{2.7}$$

in which the mass m is assumed to be unity.

According to [19], the trajectories of the particles are calculated using a Velocity-Verlet integrator with a time-step that is small enough to capture the time-dependency of the potential.

2.4.3 Neural Net

In Sec. 2.3 the general quantities of a neural network were presented. The specific network used to interpolate the DS in this work is a "feed-forward" network and contains four hidden layers consisting out of $40 \times 40 \times 40 \times 10$ neurons. The input neurons provide the values of y, v_y, and t for which the position of the NHIM shall be calculated. Given

these parameters, the output value of the output-neuron is the position x of the NHIM to which the DS is attached.

To speed up the procedure of computing the overall gradient of the cost function, the *stochastic* gradient descent method is used for the training of the network. It is trained for 50,000 epoches while a single batch contains 1,000 data points.

2.4.4 Fitting procedure

Sec. 2.1 declared what the rate constant is and how it can be estimated through a fit of the number of reactants over time. In practise, the fitting procedure is not as straight forward as it seems to be according to Fig. 2.1. For instance, the transition from the constant number of reactants during the settling time to its exponential decay is much smoother than it is in Fig. 2.1 and therefore affects a broader range of time. Since one is not interested in the settling behavior of the system, it is not useful to fit the affected time range. This decreases the size of the range of time that can be fitted.

Another problem occurs when fitting the curve of $N_\mathrm{r}(t) - N_\mathrm{r}(\infty)$ with an exponential function: reactions at the start of the fit range have a much bigger impact on the rate constant than reactions at the end of the fit range. In TST one is especially interested in particles that stay in the saddle region for a long time and therefore react at a later time of the reaction. Hence, the fit-function is chosen to be a linear function $k \cdot t$ that fits the logarithmic of the number of reactants $\log(N_\mathrm{r} - N_\mathrm{r}(\infty))$ over time, so that reactions at the beginning and at the end of the fit range are equally impacting the rate constant.

3 Numerical Estimation of Rate Constants

In a numerical simulation, the rate is influenced by various aspects, like the size of the ensemble, the distinction between reactant and product and the fitting procedure that is used to estimate the rate. This section will present some of these aspects and display in what way and to what degree they influence the rate and what can be done to estimate the rate as accurately as possible.

3.1 Recrossing Particles

It is an important requirement for the dividing surface to be recrossing-free. This means that if a particle crosses the DS it can only do so once and not multiple times, in order to prevent an overestimation of the reaction rates. However, this requirement is not entirely fullfilled for all propagations. Numerically, as well as depending on precision there is almost always a small number of recorssing particles counted. Hence, the number of recrossings represents a measurement of the accuracy of the dividing surface. Since the DS is represented by a neural net, the aim is to develop a net that provides a DS that is as free of recrossings as possible. This section will show the impact of a large number of recrossing particles on the estimation of the rate constant.

Figure 3.1 shows two plots of the population of reactants over time for two propagations of the same ensemble while using different neural nets as a representation of the dividing surface. Both ensembles propagated contain 10^6 particles positioned at $(x, y) = (-0.60, -0.56)$ and have $k_\mathrm{B}T) = 1.0$. Their propagation starts at a barrier-phase of $t_0 = 0.0$. In the first system there are 433 recrossing particles while there are only 6 in the second system. The net of the second system is used for all propagations performed in this work, see Chapter 2.3. The flat section of the curve in Fig. 3.1 at times from $t = 2.0$ to $t = 3.0$ in the first system indicates the occurance of recrossings in this interval of time. Most of the particles either react very quickly over the barrier or are reflected immediately. But some particles stay in the saddle region for longer times before they leave again to the reactant or product side. Such particles are referred to as

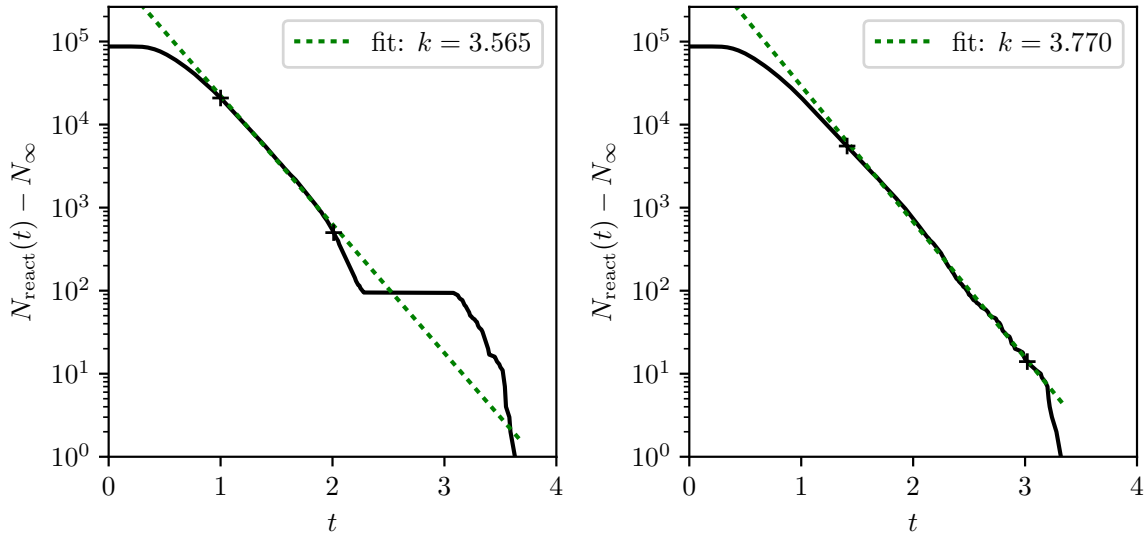

Figure 3.1: Number of reactants over time for a propagation of the same ensemble, but with a different representation of the NHIM via different neural networks. Left: poor neural network with 370 recrossings while propagating the ensemble; right: good neural network with only 6 recrossings

critical particles. These particles are most relevant in the determination of the rate constants, since they are heavily influenced by the system's dynamics. For the first system, it is not possible to estimate the reaction rate of particles that react between $t = 2.0$ and $t = 3.0$, since the related curve does not provide information about the actual rate in this interval of time. In addition, the course of the number of particles over time can not be fitted over a wide range of time because of the pertubation of the curve that is induced by recrossing particles. For the estimation of the reaction rate it is essential to have a wide fit-range that especially includes reactions at the end of the overall reaction. Rates for systems with a high number of recrossing particles are therefore more prone to uncertainties than systems with only very few recrossings. A number of six recrossings in an ensemble of 10^6 particles does not have a significant impact on the rate and does not lead to distortions. Hence, neural networks with a very low number of recrossings should be used to obtain the DS.

3.2 Fit-Range

The rate is estimated by calculating the parameter of a fit-function while the function itself is prone to uncertainties. The size as well as the location of the fitted range usually has to be chosen individually to match the course of the number of reactants over time as precisely as possible. Within one plot of the number of reactive particles over time, there are various time-ranges that are smooth and wide enough to provide a clear rate constant of the particles that react in the respective range. Fig. 3.2 shows three reaction rates over different values of the ensemble's $k_{\mathrm{B}}T$: the biggest and smallest rate that are estimated by fitting different ranges of time, as well as the rate that is obtained by fitting over the longest range of time possible while still matching the curve closely. When fitting over different ranges of time, the fit-ranges contain reactions of different kinds of particles. Roughly speaking, particles that react within the same small range of time have a similar initial kinetic energy and therefore react with a constant rate. Particles that react at a time much sooner or later than the particles mentioned above have a different initial kinetic energy and possibly a different rate as well. Fig. 3.3 shows a plot of the number of reactive particles over time, fitted with the three different fit-ranges for $k_{\mathrm{B}}T = 7.0$. It is striking, that only a small difference in the fit-curve's gradient leads to a big difference in the respective reaction rate.

The data in Figure 3.2 displays the following relation: The higher the value of $k_{\mathrm{B}}T$, the more these rates deviate from one another. In an ensemble with a high temperature $k_{\mathrm{B}}T$, the distribution of the kinetic energy is broader than that of an ensemble with a small value of $k_{\mathrm{B}}T$. Given an ensemble that contains particles whose kinetic energies differ from each other on a bigger scale, the rates are more likely to differ for different fit-ranges as well.

For an ensemble with a $k_{\mathrm{B}}T = 1.0$ the smallest rate that can be estimated is $k = 3.188$ whereas the largest rate is $k = 3.396$. When analysing rates of an ensemble with this energy it should be considered that the rates might have a deviation of approximately $\Delta k = 0.2$ due to a different fit-range.

In order to be able to compare reaction rates for various propagations it is ideal to choose the same value of $k_{\mathrm{B}}T$ as well as a similar fit-range.

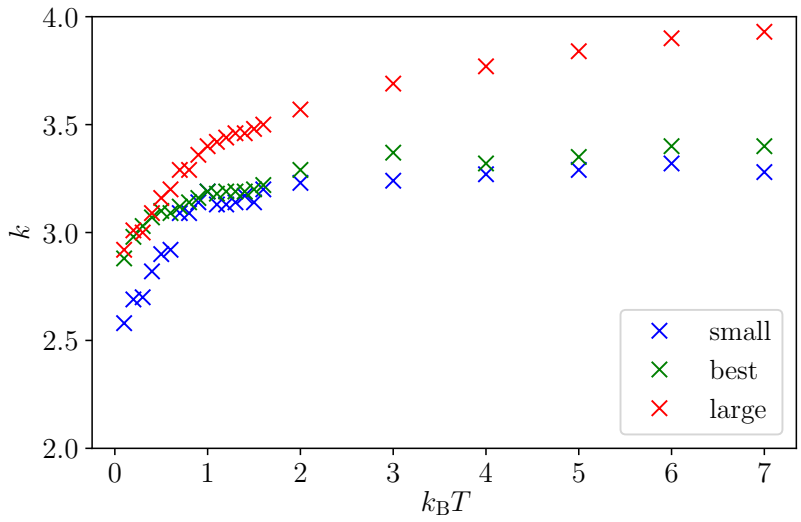

Figure 3.2: Most accurate, largest and smallest reaction rate that can be fitted vs. the ensemble's temperature. Ensemble is initially positioned at $x = -0.2$ with 10^6 particles in a static system.

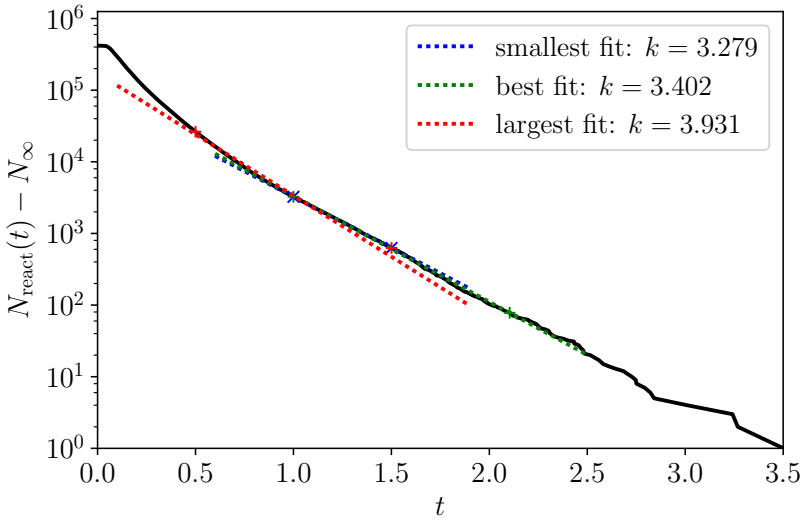

Figure 3.3: Plot of the number of reactive particles over time, fitted in three possible ranges that lead to the most accurate, the largest and the smallest reaction rate. Ensemble is initially positioned at $x = -0.2$ with 10^6 particles and a temperature $k_\mathrm{B}T = 7.0$ in a static system.

3.3 The Barrier-Phase

In a time-dependent periodically driven system, the barrier as well as the DS perform an oscillation along the x-axis while the particles are propagated. The system can be started at arbitrary phases t_0 of the oscillation within one period length. For standard settings the period length is $T = 2.0$. According to Table 3.1, the reaction rate of the propagated particles depends on the inital phase of the barrier. Further details of this relation are examined in Sec. 4.2. The following calculations compare the variance of the rate when averaged over 24 different barrier-phases and when averaged over only 8 barrier-phases chosen equidistantly in a full period T. These 8 barrier-phases are highlighted in blue in Tab. 3.1.

Table 3.1: Reaction rate k and the respective initial phase of the barrier t_0

t_0	k	$k - \overline{k}$
0.0	3.586	0.409
0.1	3.545	0.368
0.2	3.408	0.231
0.25	3.356	0.179
0.3	3.312	0.135
0.4	3.047	-0.130
0.5	2.897	-0.280
0.6	2.919	-0.258
0.7	2.935	-0.241
0.75	2.938	-0.239
0.8	2.981	-0.196
0.9	2.965	-0.212
1.0	3.010	-0.167
1.1	3.027	-0.150
1.2	3.076	-0.101
1.25	3.060	-0.117
1.3	3.147	-0.030
1.4	3.071	-0.106
1.5	3.273	0.096
1.6	3.264	0.087
1.7	3.330	0.153
1.75	3.341	0.165
1.8	3.304	0.128
1.9	3.452	0.275
average rate: $\overline{k} = 3.177$		

$$\sigma = \sqrt{\frac{1}{n}\sum_{\mathrm{i}=1}^{n}(k_\mathrm{i} - \overline{k})^2}$$

$$\sigma_\mathrm{all} = \sqrt{\frac{1}{24}\sum_{\mathrm{i}=1}^{24}(k_\mathrm{i} - 3.177)^2} = 0.205$$

$$\sigma_\mathrm{blue} = \sqrt{\frac{1}{8}\sum_{\mathrm{i}=1}^{8}(k_\mathrm{i} - 3.195)^2} = 0.206$$

The data in Table 3.1 refers to the rates of an ensemble initially positioned at $(x, y) = (-0.60, -0.56)$ and with $k_{\mathrm{B}}T = 1.0$. The system is dynamic and the potential's parameters are set to the standard values.
The respective variance of the rates differs by only 0.01. For ensembles with different properties, the course of the dependence of the rate on the barrier's phase can vary. In order to be able to calculate reaction rates that can be compared for different systems, one can average each rate for different initial phases of the respective barrier. When averaging over 24 instead of only 8 barrier phases, the difference in the rate is 0.2. Averaging over a bigger number of barrier-phases generally gives an average rate with a higher accuracy. To obtain reaction rates of a system with various initial barrier-phases, the simulation has to be reapeated for each setting. For the sake of saving disk space and computational time, we from now on only average over 8 barrier-phases (referred to as the "average rate"), as the variance still is not very different from the 24 sample cast.

3.4 Dividing Surface of a Static System

When starting a propagation of particles at different initial barrier-phases in a static system ($\hat{x} = 0.0$) one expects to obtain the same reaction rate for all phases, because the phase-variation has no effect on the potential $V(x, y, t)$, since

$$\begin{aligned} V(x,y,t)_{\hat{x}=0.0} &= E_b \, \exp(-a[x - \hat{x} \, \sin(\omega_x \, t)]^2) + \frac{\omega_y^2}{2} \, [y - \frac{2}{\pi} \, \hat{y} \arctan(\tilde{a} \, x)]^2 \\ &= E_b \, \exp(-a \, x^2) + \frac{\omega_y^2}{2} [y - \frac{2}{\pi} \, \hat{y} \arctan(\tilde{a} \, x)]^2 \quad , \\ \frac{\partial V(x,y,t)_{\hat{x}=0.0}}{\partial t} &= 0 \quad . \end{aligned}$$

However, the rates slightly differ from one another. Table 3.2 presents the reaction rates of a static system for the ensemble of the previous section for 8 different barrier-phases equally distributed within one period of the barrier's oscillation. The following calculation determines the rate's variance.

Table 3.2: Reaction rate k for the respective initial phase of the barrier t_0

t_0	k	$k - \overline{k}$
0.0	3.056	0.011
0.25	3.032	-0.013
0.5	3.053	0.008
0.75	3.033	-0.012
1.0	3.059	0.014
1.25	3.034	-0.011
1.5	3.06	0.014
1.75	3.035	0.010
average rate: $\overline{k} = 3.045$		

$$\sigma = \sqrt{\frac{1}{8}\sum_{\mathrm{i}=1}^{8}(k_{\mathrm{i}} - 3.045)^2} = 0.012$$

The variance of the rate is 0.012, which is six percent of the rate's variance for a dynamic system and therefore relatively small. When starting the propagation at a barrier-phase of t_0, the DS will be evaluated from that time onwards. In a static system for which the amplitude of the barrier's oscillation is set to zero, this is the only impact a different initial barrier-phase has. Since the DS is interpolated by the neural net, if the DS changes in time the interpolation of the neural network has to be assumed to be inaccurate. When looking at a dynamic system, the deviation of the rates due to this inaccuracy has to be added to the deviation due to the barrier's movement.
However, this additional deviation can be eluded when there is simply no time range given for the interpolation of the DS by the neural network.

3.5 Effects of the Ensemble's Size

According to Sec. 2.4, the total energy of the ensembles used in this work usually follows a Maxwell-Boltzmann distribution. The kinetic and potential energies of a particle are obtained by sampling the outputs of a random-number generator according to the distribution. The random-number generator requires an arbitrary number for initialization, a so-called "seed". This seed can be varied for each propagation. Changing the seed leads to a slightly different energy distribution of the ensemble's particles. The deviation of two ensembles that are generated with a different seed can be expected to converge to zero for a large number of particles. The standard ensemble in this work contains a total number of 10^6 particles. Since this is a high amount of particles it seems unlikely to

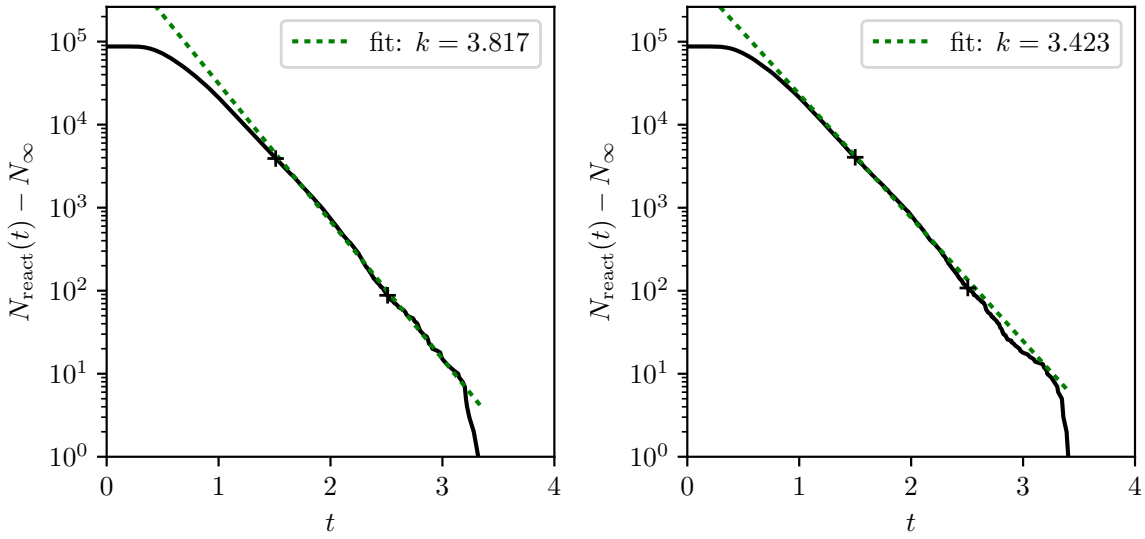

Figure 3.4: Number of reactive particles over time for two ensembles generated with a different seed fitted with the same range from $t = 1.5$ to $t = 2.5$. Left: ensemble generated with a seed $S = 13$. Right: ensemble generated with a seed $S = 100.0$.

observe any differences of ensembles with a different seed. However, when propagating various ensembles that solely differ in the value of the seed that was used to generate their energy distribution, the reaction rates as well as the number of recrossing particles can differ. For a seed of 50 there are 3 recrossing particles whereas there are 6 for a seed of 13. Table 3.4 displays the reaction rate of an ensemble for 12 different seeds. In the first column, the fit-range in the plot of the number of reactants over time remains unchanged for all seeds. The reaction rate fluctuates by up to 0.394. The variance of these rates is

$$\sigma_{\text{uniform}} = \sqrt{\frac{1}{12}\sum_{\text{i}=1}^{12}(k_{\text{i}} - 3.608)^2} = 0.094 \quad .$$

A variance of $\sigma_{\text{uniform}} = 0.094$ that is solely due to a variation of the seed, is a reflection of the system's sensitivity to small deviations in the ensemble and therefore underlines the critical behavior of and on particles staying in the saddle region for longer times. Fig. 3.4 shows two plots of the number of reactive particles over time, fitted with the same fit-range for two ensembles that were generated using a different seed. One can observe slight differences in the course of the two curves that lead to a significant difference in

Table 3.3: Reaction rate k fitted with a uniform and an adjusted fit-range for an ensemble generated with a seed S.

S	k for a uniform-fit-range	k for adjusted fit-ranges
4	3.564	3.564
10	3.527	3.527
13	3.817	3.646
20	3.563	3.563
30	3.570	3.570
40	3.719	3.629
50	3.621	3.621
60	3.632	3.632
70	3.591	3.636
80	3.612	3.612
90	3.661	3.661
100	3.423	3.581
	$\overline{k} = 3.608$	$\overline{k} = 3.603$

the reaction rates. It should be noted that the number of particles that react within the fit-range and therefore determine the rate hardly make up 1% of the total number of particles in the ensemble. Despite the fact that the distribution of these particles varies for different seeds, the overall distribution could still be seen as independent of the seed. By adjusting the fit-range in a way that the fit matches the curve of the number of reactive particles over time as closely as possible, one can counteract the seed's impact on the rates. The third column in Table 3.3 displays the reaction rate obtained by individually adjusting the fit-ranges of plots in which the deviation of the fit with the uniform fit-range and the curve itself was clearly visible. The following calculation determines the variance of the rates for adjusted fit-ranges:

$$\sigma_{\text{adjusted}} = \sqrt{\frac{1}{12}\sum_{\text{i}=1}^{12}(k_{\text{i}} - 3.603)} = 0.039 \quad .$$

The variance of the rates is less than half the variance obtained for fitting all plots with the same fit-range. When comparing reaction rates of different systems in this work the seed remains unchanged. However, to actually decrease the statistical error, it would be best to simulate with a higher number of particles and especially increase the number of reactions that are taken into account for the fit. Since this would make the simulation much more time consuming, it was not possible to increase the number of particles in this work.

4 Calculating Reaction Rates with a Suitable Ensemble

4.1 Obtaining a Suitable Ensemble

The reaction rate regarding the barrier's dynamics ought to be independent of the ensemble's properties such as its position in the two-dimensional (x, y)-space. However, this independence can not be observed for every ensemble. In this chapter it is clarified for what kind of ensemble this requirement is fulfilled and for what kind it is not.

The first ensemble that is investigated has a fixed position on the x-axis but is expanded in y-direction. For numerical reasons, the values of y are restricted to a range from -10 to 10. The ensemble's position can be visualised as a slice of particles in y-direction. Both velocities v_x and v_y are also restricted to a range from -10 to 10 and the value of $k_\mathrm{B}T$ is set to 3.0.

Fig. 4.1 displays the averaged reaction rate of the above mentioned ensemble at different positions along the x-axis. From $x = -0.5$ to $x = 0$ the rate increases exponentially and is almost constant for positions from $x = -2.0$ to $x = -0.4$. In order to identify the cause of this exponential dependence, the energy distributions of the ensemble at the different initial positions are examined. The total energy of an ensemble at a given x-position is the sum of the kinetic and the potential energy of its particles. The potential energy for a particle at a certain position is given by the energy of the potential at this position. The potential is not constant along the x-axis and has a high increase for values from $x = -1$ to $x = 0$. An ensemble at $x = -0.1$ has a remarkably higher potential energy than it does at $x = -2.0$. The potential energy of a particle determines its likelihood to react. When it is rather low it is only possible for particles with a high kinetic energy to cross the dividing surface and react. As a consequence, the share of reactive particles in the ensemble at $x = -0.1$ is approximately 33 % whereas the percentage of reactive particles is only 13 % in the ensemble at $x = -2.0$. One of the graphs in Fig. 4.2 shows the share of the number of reactive particles in the ensemble that is expanded in y-direction for x-positions from -0.1 to -2.0. The effect of the high increase of the potential's energy on the number of reactive particles is clearly visible in a range from $x = -1$ to $x = 0$. Later in this section it will be clearified whether this relation could be the cause of the rate's increase for x-positions closer to the barrier. Regardless of the difference in the potential

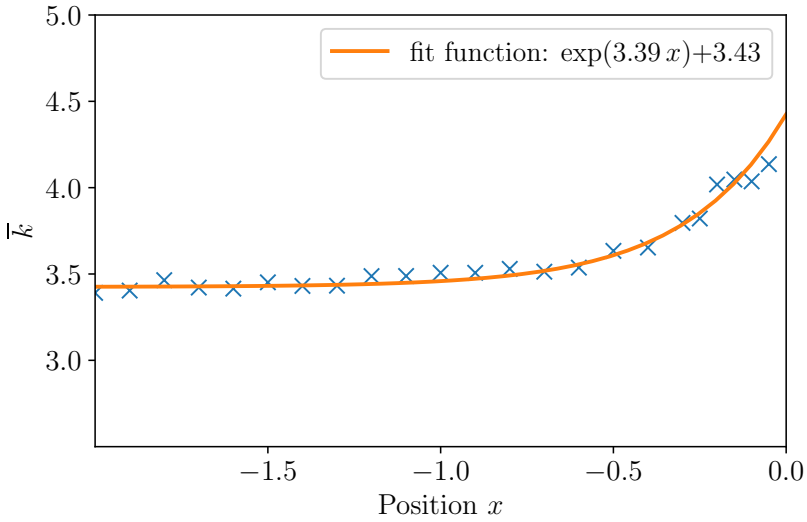

Figure 4.1: Averaged rates of the reaction of an ensemble expanded in y-direction and $k_\mathrm{B}T = 3.0$ located at different initial positions in x-direction. The data is fitted with an exponential function. The potential is time-dependent with the standard parameters.

energies of ensembles positioned along the x-axis, they all have the same overall kinetic energy which otherwise could have an effect on the rate. Within an ensemble the kinetic energy of a particle does in fact depend on its potential energy which changes along the y-axis. Particles that are positioned further away from the position that has the lowest potential energy have a much higher potential energy than the ones close to it due to how the potential is defined. Due to the distribution of the total energy, particles with a high potential energy are more likely to have a small kinetic energy. The higher the value of $k_\mathrm{B}T$, the bigger the amount of particles positioned at y-positions with high potential energies. As a $k_\mathrm{B}T$ of 3.0 is relatively big, the accurance of these kinds of particles can not be neglected and must be kept in mind. When propagating particles with an initial position at a high potential energy, they are likely to perform oscillations along the parabolic potential in y-direction. For the cases in which the particles have a positive initial velocity it is possible to cross the dividing surface. It can be assumed that they cross with a high velocity after accelerating during their oscillation in y-direction. Since the rate is a quantity of how fast a particle crosses the dividing surface, this behavior would lead to an increase of the rate. The closer such an ensemble is positioned to the barrier's top, the smaller the velocity in positive x-direction must be in order for particles with a high potential energy to react. Therefore, there are more particles that lead to an increase of the rate for ensembles with x-positions closer to zero. This relation is consistent with what is observed in Fig. 4.1.

In order to confirm the hypothesis about particles with high potential energies, another

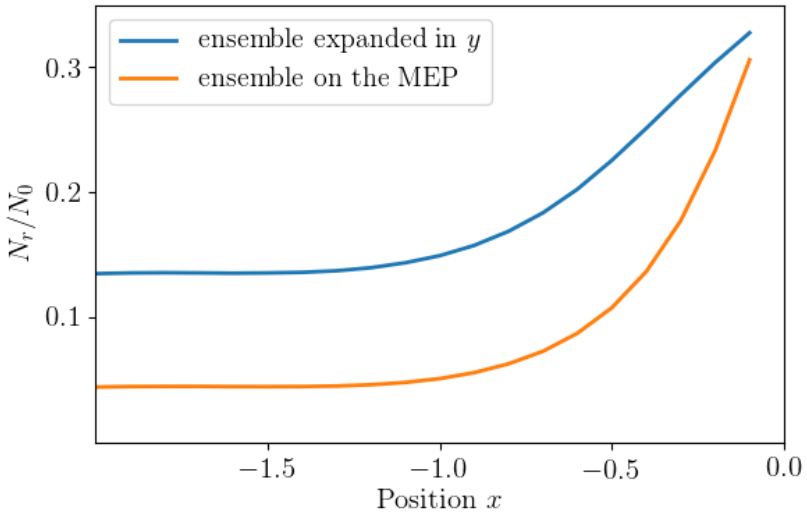

Figure 4.2: Share of the number of reactive particles N_r in two ensembles each containing $N_0 = 10^6$ particles vs. the ensembles' respective positions along the x-axis. Blue: ensemble with a temperature $k_\mathrm{B}T = 3.0$ and an expansion in y-direction; Orange: ensemble with a temperature $k_\mathrm{B}T = 1.0$ positioned on a point on the MEP.

ensemble with y-positions within a restricting range of (-0.25, 0.25) is propagated at a position of $x = -0.2$ where their effect on the rate is noticable. Having cut out most of the particles with possibly fast reactions, one expects a decrease of the rate up to $k \approx 3.5$, as it is the case for ensembles that are positioned at $x = -2.0$ to $x = -1.5$. Fig. 4.3 shows a plot of the number of reactive particles over time including the fit-function for an ensemble with a y-value with a restricting range of $(-10, 10)$ and an ensemble with y-values that do not exceed the range $(-0.25, 0.25)$. Both ensembles have initial positions at $x = -0.2$ and are propagated at a barrier-phase $t_0 = 0.0$. It is not necessary to average over the barrier's phase for the purpose of comparing the rates because the ensembles have the same x-position (for further explanation, see Sec. 4.2). The rate of the ensemble with a larger y-range has a reaction rate of $k = 4.022$ whereas the one with the much smaller range has a rate of $k = 3.563$ which is consistent with what was expected. This leads to the conclusion that the particles located at positions of high potential energy can in fact react with a high velocity and cause an increase of the reaction rate. Having particles with velocities higher than a certain value does not serve the purpose of calculating a reaction rate that is determined by the barrier's movement. These particles cross the dividing surface without being affected by the potential's dynamics which will be elaborated in the following section. In TST one is especially interested in the so-called "rare event" in which a particle has just as much energy as it needs to overcome the barrier. The reaction rate of such particles is the

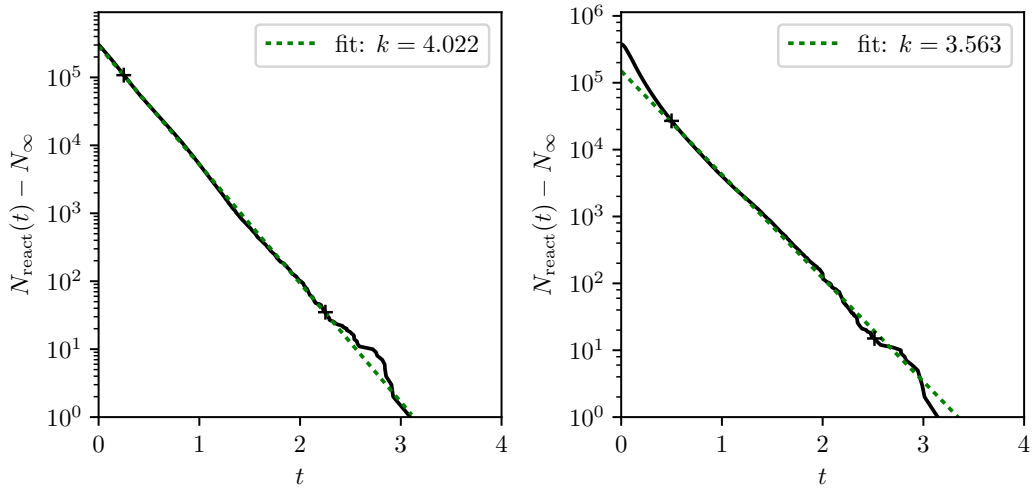

Figure 4.3: Plot of the number of reacting particles over time at a barrier phase $t_0 = 0.0$ for ensembles with a different expansion in y-direction. Left: Ensemble with y-positions within a restricting range of $(-10, 10)$; Right: ensemble with a restricting y-range of $(-0.25, 0.25)$.

crucial rate in TST. Therefore, it is best to position the ensemble at the path of minimum energy in the potential. For a given x, the corresponding y-position on the MEP which has the smallest potential energy can be calculated with Eq. (2.5).

Figure 4.4 shows the averaged rates of an ensemble that is positioned along different x-positions directly on the MEP. The value of $k_\mathrm{B}T$ is set to 1.0 which leads to a smaller reaction rate. The cause of this effect will be elaborated in the following section. The rate in Fig. 4.4 can be seen as constant among all x-positions within the overall imprecision. Concentrating all of the ensemble's particles in a single point has clearly eliminated the rate's dependence on the ensemble's position.

Similar to the course of the share of reactive particles of an ensemble expanded in y-direction in Fig. 4.2, the course of the share of reactive particles of the ensemble on the MEP also increases expontentially for x-positions near the barrier's top. The only difference is that the number of reactants for the ensemble with a $k_\mathrm{B}T = 1.0$ at $x = -2.0$ is much smaller than for the one with $k_\mathrm{B}T = 3.0$. This effect will be dealt with in the Sec. 4.1.1 and is not caused by the difference in the y-range but by the difference of $k_\mathrm{B}T$. Hence, it can be assumed that the number of reactive particles is decreasing in a similar way for both kinds of ensembles. Still, one ensemble has a constant reaction rate among different x-positions while the other one has rates that depend on its x-position. Therefore, the decrease of reactive particles in Fig. 4.1 is not likely to be the cause of the rate's dependence on x. In conclusion, it seems that the particles with high potential energies in an ensemble with a large y-range are the sole cause of the rate's dependence

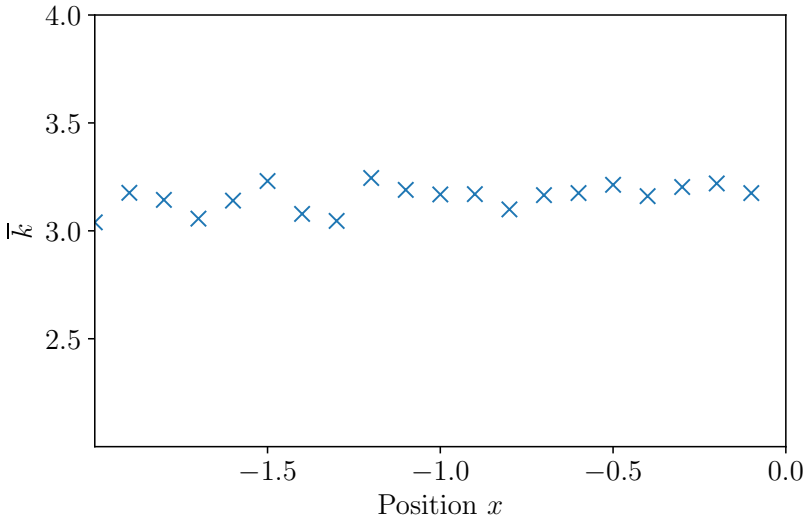

Figure 4.4: Averaged reaction rates of the ensemble with $k_\mathrm{B}T = 1.0$ located at different initial x-positions on the MEP. The potential is time-dependent with the standard parameters.

of the ensemble's position x. Hence, the ensemble will always be positioned on the MEP for all following propagations.

4.1.1 Optimization of the Ensemble's Energy

In order to determine a rate that provides information about the system's dynamics close to the saddle, it is necessary to generate an ensemble containing a high amount of particles that will stay in the saddle region preferably for many oscillations. This section deals with the task to find the optimal kinetic energy for which the ensemble contains sufficient share of critical particles.

Particles with a very large kinetic energy compared to the barrier height pass the dividing surface without being affected much by the dynamics of the potential. As a result, the reaction rate is mostly a property of the ensemble itself and does not correspond much to the rate due to the barrier's composition and movement. In contrast, particles with a kinetic energy lower than a certain value do not reach the dividing surface and do not react at all. For this reason, the kinetic energy of an ensemble can not be chosen arbitrarily.

Figure 4.5 displays the number of reacting particles over time in a static as well as in a dynamic system. The amplitude of the barrier's movement in x-direction which is described by the parameter $\hat{x}$ is 0.0 for a static system whereas it is 0.4 for a dynamic

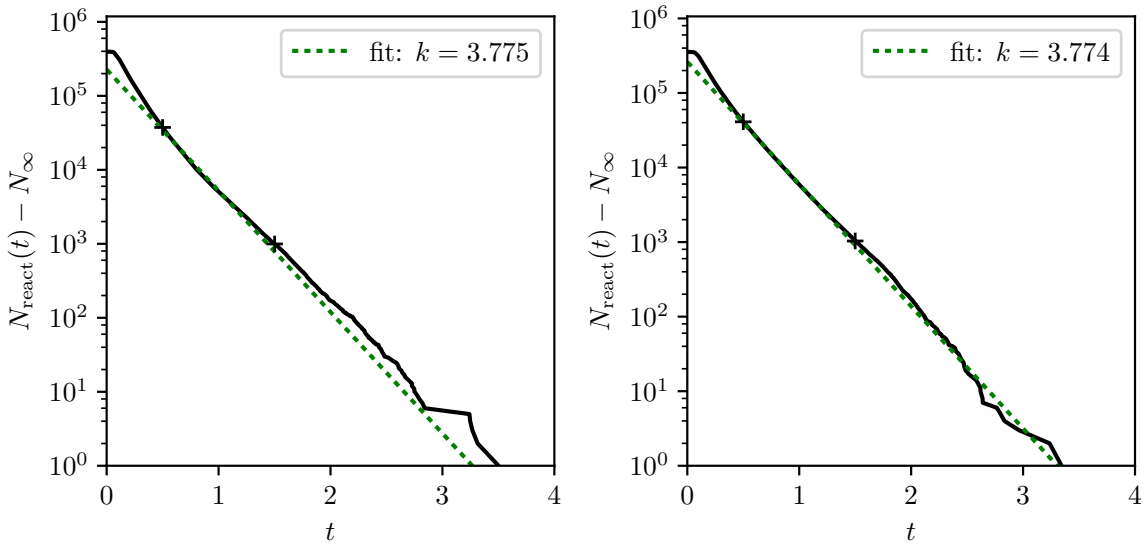

Figure 4.5: Number of reactive particles over time for two different potentials fitted within the same time-range. Left: static potential with $\hat{x} = 0.0$ and a rate $k = 3.775$. Right: dynamic potential with $\hat{x} = 0.4$ and a rate $k = 3.774$.

system. In both cases the ensemble's value of $k_\mathrm{B}T$ is 4.0, which is far above the barrier height that has a value of $E_\mathrm{b} = 2.0$. Since the total number of reactants is kept constant, the ensemble has a higher concentration of relatively fast particles and a lower concentration of slow ones compared to an ensemble with a smaller value of $k_\mathrm{B}T$. Both ensembles are located at $x = -0.2$ and on the minimum energy path of the potential. Fast particles are likely to pass the dividing surface shortly after the propagation has started. Their reactions are found at the beginning of the overall reaction. Therefore, the fitting ranges in both plots are not chosen to match the curves as closely as possible but to give a reaction rate of only the faster particles of the ensemble. The rates displayed in Fig. 4.5 are equal and do not show a dependence on the potential's properties. This coherence indicates that the fast particles of an ensemble with $k_\mathrm{B}T = 4.0$ are not affected by the barrier's movement, despite having converted kinetic into potential energy while moving towards the barrier. As it can be seen in Fig. 4.5, the fast particles that react at the beginning of the overall reaction make up most of the reacting particles. In order to have a significant amount of critical particles, these particles must as well be slow enough to be affected by the potential. Consequently, the value of the optimal $k_\mathrm{B}T$ must be smaller than 4.0.

Figure 4.6 shows the reaction rate of the fast particles of the respective ensemble over values of $k_\mathrm{B}T$ between 0.0 and 7.0 for a static and a dynamic potential. For $k_\mathrm{B}T > 1.5$ the two graphs converge into one. The difference in the system's dynamics does not manifest

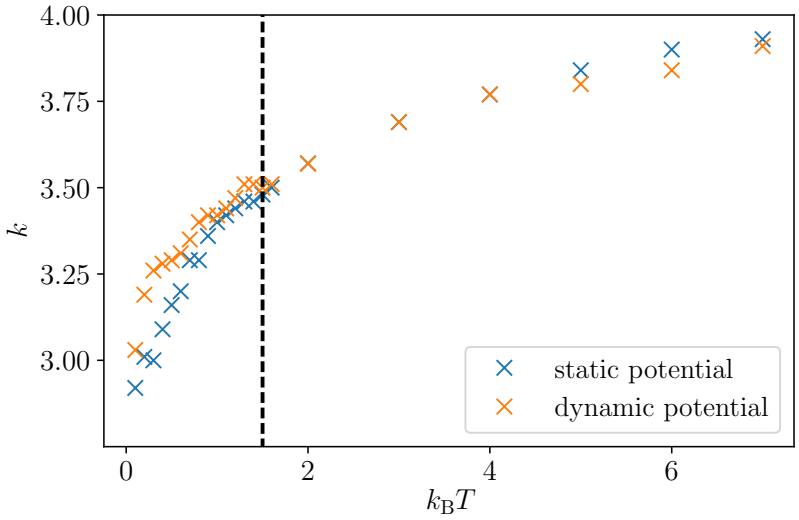

Figure 4.6: Reaction rates of the fastest particles of an ensemble with various values of k_BT for a static and a dynamic potential. The line at $k_BT = 1.5$ marks the value of k_BT for which the two graphs converge into one.

itself in the reaction rate once $k_BT = 1.5$ is exceeded. For all values of $k_BT < 1.5$ the rates show larger values for a dynamic potential and therefore provide information about the influence of the barrier's movement. This dependence of the rates on different sets of parameters will be confirmed in Sec. 4.4. It should be noted that these rates are not averaged for various barrier-phases and are not the result of the most accurate fitting, but of the fitting of the fastest particles and are therefore slighty higher than the rates obtained via optimal fitting for the same set of parameters.

Figure 4.7 shows the increase of the number of reactants for higher values of k_BT in a static system. The total number of particles in the propagated ensemble is $N = 10^6$. For small k_BT the share of reactive particles increases rapidly and afterwards converges to a number slightly above 40 % at $k_BT = 7.0$. Approximately half of the particles have a velocity in negative x-direction and are not likely to reach the barrier's top. A percentage of reacting particles of 40 % means that roughly 80 % of all particles that were initialized with a positive velocity in x-direction are reactive particles. At the much smaller value of $k_BT = 1.0$ the percentage of the above mentioned particles is around 60 %. For the purpose of obtaining a smooth plot of the reactive particles over time that leads to a clear reaction rate, this is a sufficient share of reactive particles.

In conclusion, an ensemble with $k_BT = 1.0$ contains a high amount of critical particles while still having an adequate percentage of reacting particles. For all following calculations in this chapter, the value of k_BT will be set to 1.0.

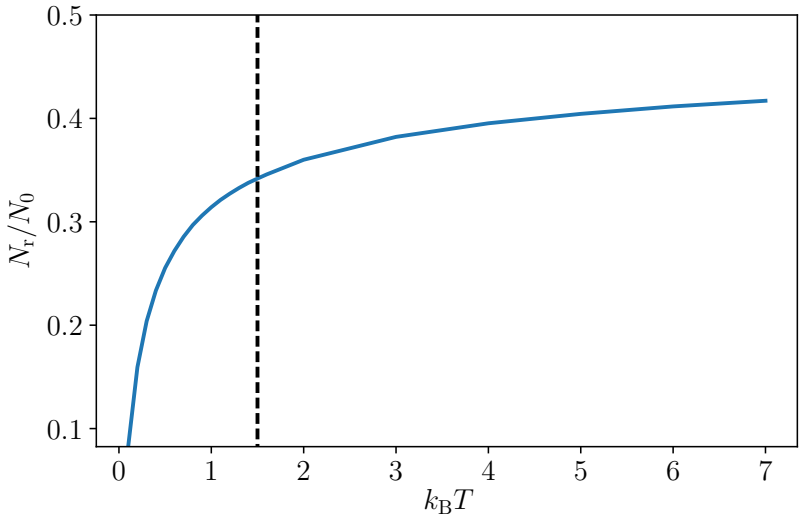

Figure 4.7: Share of reactive particles $N_{\text{react.}}$ in the ensemble containing N_0 particles vs. the value of k_BT for a static system.

4.2 Dependence of the Rate on the Barrier-Phase

When calculating reaction rates that reflect the system's dynamics, one has to take into consideration that these rates are influenced by the barrier's movement at the time at which the individual particles react. This section deals with the question of how the barrier's phase influences the reaction rate as well as the number of reacting particles. The barrier-phase t_0 refers to the phase of its oscillation at which the propagation of the particles starts. The relation between barrier-phase and reaction rate will be examined for two ensembles on the minimum-energy-path with a $k_BT = 1.0$. One ensemble is positioned at $x = -0.4$ whereas the other one is positioned at $x = -0.8$. The parameters of the potential are set to the standard values with a period length of $T = 2.0$.

The upper plot in Fig. 4.8 displays the dependence of the rate on the barrier's phase for both ensembles as well as the respective averaged rate over all phases. The fitting range of the exponential decay of reactive particles for the ensemble at $x = -0.4$ is $t = (0.8, 1.8)$. For the ensemble at $x = -0.8$ this range is set to be $t = (1.2, 2.2)$. As it was shown in Sec. 4.1, given an ensemble at the minimum-energy-path, the different positions of the ensembles do not influence the average rate in a significant way. Here, the average rates only differ from each other by a value of 0.01, which is significantly smaller than the other errors discussed in Chapt. 3 and can be neglected. However, for different phases within one period of the barrier's oscillation, the rates differ up to a value of 0.75. Both ensembles show a similar pattern in the dependence of the rate on the barrier's phase. They are relatively big for initial phases t_0 at the beginning and

the end of a period and have a minimum inbetween. The minima of both ensembles are at a barrier-phase of $t_0 = 0.8$. However, the range in which the rates are smaller than the average rate is broader for the ensemble at $x = -0.4$ and the center of this range is at approximately $t = 1.1$, whereas it is at $t = 0.9$ for the ensemble at $x = -0.8$. This shift of 0.2 indicates that the particles that are taken into account fitting the rate need a time of roughly 0.2 to move from $x = -0.8$ to $x = -0.4$. Therefore, the mean velocity of the particles starting at $x = -0.8$ can be estimated to be $\overline{v} = 2.0$. It should be noted that the velocity can not be seen as constant because the particle's kinetic energy is converted into potential energy as they move towards the barrier's top.

In order to determine what causes the correlation between the reaction rate and the barrier's phase, a connection between the rate and the phase of the dividing surface at the moment of reaction must be found. The barrier is in phase with the dividing surface but has a bigger amplitude. Since the dividing surface is attached to the NHIM, it is moved along with the NHIM's oscillation. Fig. 4.9 displays the oscillation of the NHIM for two periods.

First, the DS's movement for the initial barrier-phase that leads to the minimum rate is analysed. As mentioned above, for the ensemble at $x = -0.4$ the minimum rate is at $t_0 = 0.8$. In this case, the fitting of the rate starts at a time of $t = 0.8 + 0.8 = 1.6$. The particles that react at the beginning of the fitting range at 1.6 cross the dividing surface when it is at the reversal point of its oscillation and has an amplitude of -0.13. The particles that react at the end of the fitting range at $t = 2.6$ at which the dividing surface is at the reversal point at $x = +0.13$. Particles that react within this fitting range react while the DS is constantly moving away from them which seems to lead to a minimum value of the rate. In contrast, when starting the propagation at a barrier-phase of $t_0 = 1.8$, the particles resposible for the rate react at times from $t = 2.6$ to $t = 3.6$. In this range of time the DS is moving towards the particles (highlighted in red in Fig. 4.9). In this case the reaction rate is above the average rate. Through the comparison of the DS's movement for the minimum and maximum reaction rate, it can be assumed that the DS's direction of movement has a direct impact on the rate. The cause of this impact is likely to be the different relative velocities of the DS and the particles. When the barrier is moving away from the particles, the relative velocity is small and vice versa. Since the rate is a quantity of how fast the particles cross the DS, it is proportional to their relative velocity. The relative velocity is especially big when the DS has a high velocity towards the ensemble. In addition, particles that react while the barrier is moving away from them lose more kinetic energy while moving towards the DS, since the DS has already moved forward as soon as the particles have overcome the potential energy of their previous position. This is the case because the the DS has already moved forward as soon as the particles have overcome the potential energy at their previous positions. As a consequence they have a smaller velocity when reaching the DS compared to the particles reacting while the barrier is moving towards them. This increases the effect the barrier's direction of movement has on the rate.

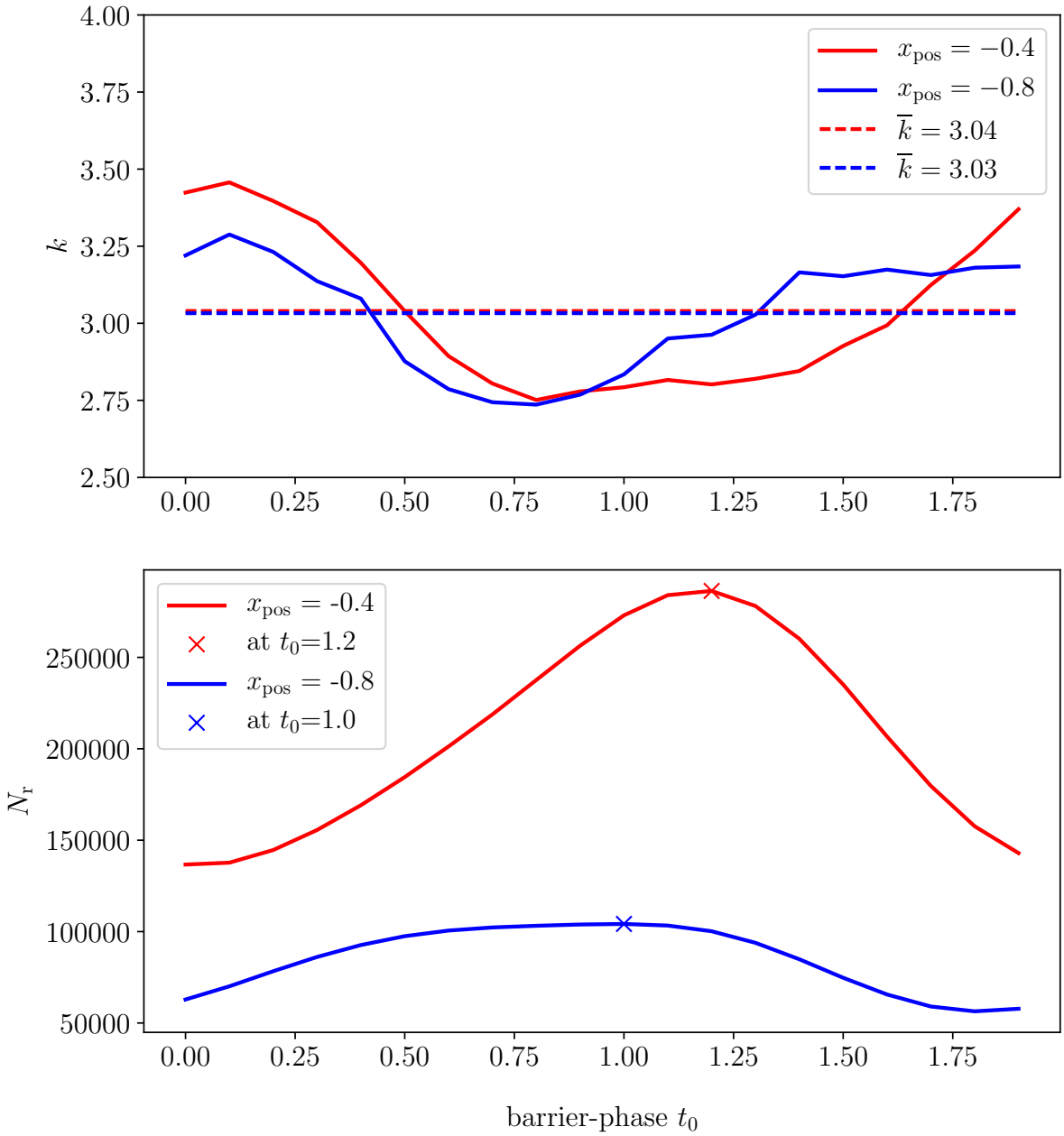

Figure 4.8: Upper plot: Reaction rate vs. the barrier-phase for two ensembles initially positioned at different x.; Lower plot: Number of reactive particles vs. the barrier-phase for two ensembles positioned at different x.

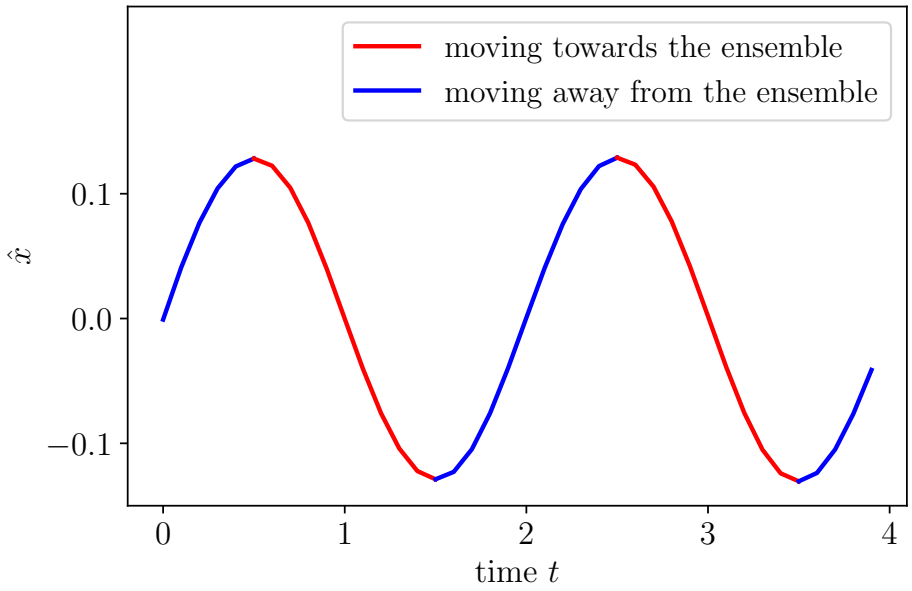

Figure 4.9: Amplitude of the oscillation of the NHIM for **two** full periods. Phases in which the NHIM is moving towards the ensemble are highlighted in red; phases in which the NHIM is moving away from the ensemble are highlighted in blue.

As mentioned above, the rate reaches a maximum when the DS is moving towards the ensemble and minimal when it is moving away from the ensemble. Therefore, one expects these two contrary effects of the DS's movement to compensate each other, when the amount of time spent moving towards the ensemble and away from the ensemble is equal within the fit-range. However, it can be observed that the impact of the DS's movement is mainly determined by its movement at the beginning of the fit-range rather than by its movement at the end of the fit-range. For expample, for a barrier-phase of $t_0 = 0.3$ the particles that react at the beginning of the fit-range react while the barrier is moving towards them while the particles reacting at the end of the same fit-range react while the barrier is moving away from them. This circumstance results in a reaction rate larger than the average rate, which indicates that the rate of the particles reacting at the beginning of the fit range has a bigger impact on the overall rate. For a barrier-phase of $t_0 = 1.3$ these particles react while the barrier is moving away from them which leads to a smaller rate. Consequently, the reaction rate for a system that starts at $t_0 = 0.3$ is bigger than the one for a system with $t_0 = 1.3$.

The lower plot in Fig. 4.8 shows how the barrier's phase affects the number of reactive particles in both ensembles. The ensemble that has an initial position of $x = -0.4$ contains a maximum number of reactive particles of approximately three times the number

of the ensemble with an initial position of $x = -0.8$. Particles that start at $x = -0.8$ move towards the barrier until they reach $x = -0.4$ while constantly converting kinetic energy into potential energy. Thus, only particles with a positive velocity in x-direction over a certain value are able to reach the DS. Compared to the particles that start at a position of $x = -0.4$, these particles make up a smaller share of their respective initial ensemble. In addition, the ensemble at $x = -0.4$ is likely to have a broader distribution of the kinetic energy of the particles that reach the DS compared to the ensemble at $x = -0.8$, since also particles with a relatively small kinetic energy have the ability to reach the DS. It should also be noted that particles initialized closer to the barrier's top have a higher potential energy, making them more likely to have enough energy to react. This causality explains why the number of reactive particles is much smaller for an ensemble starting further away from the barrier's top.

For the ensemble at $x = -0.4$, the maximum number of reactive particles is reached at a barrier's phase of $t_0 = 1.2$. The lowest number of reactive particles is at $t_0 = 0.0$. In order to explain this behavior, the barrier's position and movement to the beginning of the propagation for the different values of t_0 must be analysed, since roughly 70% to 90% of all reactants react within a range from $t = 0.3$ to the start of the fit at $t = 0.8$. The particles that react within that range of time are likely to have a higher kinetic energy than the particles that cross the DS at a later time. Therefore, they are less likely to be affected by the barrier's movement as much as the particles that react at a later time. However, the barrier's position could have an impact on the number of reactions. For an initial barrier-phase of around $t_0 = 0.0$ the distance between the initial position of the ensembles and the barrier reaches a maximum during the time-range that holds the most reactions. Here, the number of reactions is minimal. For an initial barrier-phase of around $t_0 = 1.0$ the barrier is closest to the initial position of the ensemble during that range of time. Another factor with the ability to influence the number of reactions is the position of the ensemble on the barrier for different barrier-phases. For an initial barrier-phase of $t_0 = 1.2$ the barrier is closer to the ensemble than it is for a barrier-phase of $t_0 = 1.0$ which leads to a high potential energy of the particles and makes them more likely to react. This could be a possible cause for the shift of the maximum to the barrier-phase of 1.2. The time-range that holds the most reactions for the ensemble at $x = -0.8$ is from 0.5 to 1.0. This shift of 0.2 from the respective time range of the ensemble at $x = -0.4$ leads to a shift of 0.2 of the minimum to a value of $t_0 = 1.8$.

4.3 The Ensemble's Total Number of Particles

As it was already observed for different seeds of the random number generator used to generate an ensemble in Sec. 3.5, a small number particles in an ensemble is prone to errors. When the propagated ensemble contains a larger amount of particles, the plot of

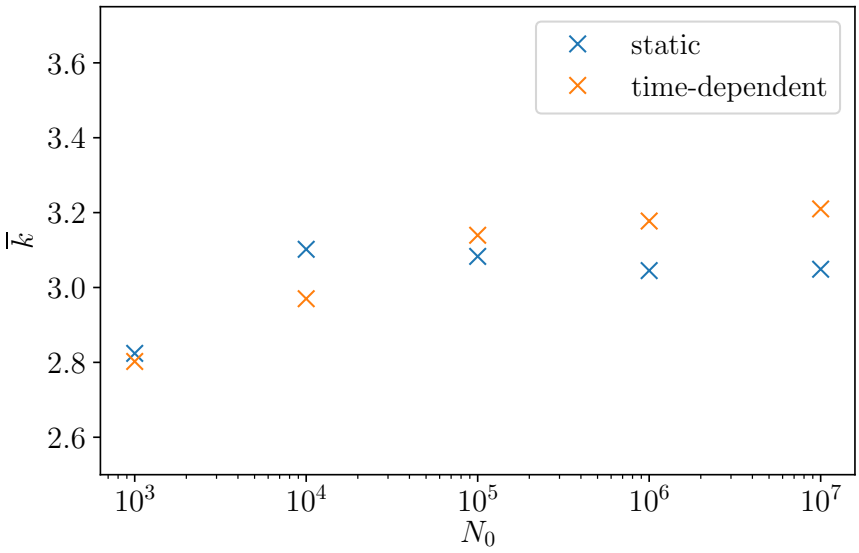

Figure 4.10: Averaged rate $\overline{k}$ vs. the total number of particles in the ensemble N_0 for a time-dependent and a static potential.

the number of reactions over time is less sensitive to fluctuations and leads to a clearer estimation of the reaction rate. Since each particle's trajectory must be evaluated separately in order to obtain the number of reactive particles over time, the computation time increases approximately linearly with the number of propagated particles. Therefore, it is favorable to propagate the least amount of particles while still obtaining a clear reaction rate with only a small deviation due to fluctuations. Figure 4.10 shows the averaged reaction rate for an increasing number of particles in the ensemble within a range from $N = 10^3$ to $N = 10^7$ for systems with a static as well as a dynamic potential. Due to physical limitations of the ITP1 workstations, it is not possible to propagate $N = 10^8$ particles at once. Both graphs in Fig. 4.10 show a convergence of the rate for an increasing amount of particles. Since the reaction rate is not significantly different for $N = 10^6$ and $N = 10^7$ and the computation time is ten times longer for the system of 10^7 particles, all of the ensembles propagated in this chapter contain 10^6 particles.

4.4 Modification of the Potential's Parameters

In this section, it is investigated how the rate is influenced by the specific structure and dynamics of the potential. For this purpose, an ensemble on the MEP at $x = -0.6$ and with a $k_\mathrm{B}T = 1.0$ is propagated. Since, for the purpose of analysing a time-dependent system, the dynamic properties of the system are of particular interest, the parameters

$\hat{x}$ and ω_x in Eq. (2.4) are varied to change the oscillation of the potential. When varying these parameters, the aim is to find resonance effects that lead to an increase of the reaction rate. In addition, the height of the barrier E_b is varied to determine how the value of the barrier's maximum energy influences the reaction rate. Lastly, the parameter $\hat{y}$ is varied in order to clarify if the distance of the potential's minima in y-direction has an impact on the rate.

Preferably, the averaged rate would be estimated for many more values of the parameters to get a more accurate impression of the respective parameter's influence on the reaction rate. However, for the determination of only a single averaged rate for a specific parameter value several steps have to be taken: the generation of training-data for the neural net, the training of the neural net with this training-data, the generation of the ensemble, the propagation of the ensemble, the estimation of the rate via the fitting procedure, the averaging of the rate over 8 different barrier-phases. So since the estimation of one averaged reaction rate is quite time-consuming, the averaged rate is only estimated for 5 to 9 different values of the respective parameters.

Fig. 4.11 shows the course of the reaction rate over the values of E_b from 1.0 to 3.0. Within the barrier height's variation range, the average rate increases linearly from a value of $\overline{k} = 2.1$ to a value of $\overline{k} = 4.1$. A possible explanation of this behavior is that only the fastest particles have enough energy to react over a higher barrier, leading to a reaction rate that is primarily a reflection of the particles high velocity. In order to verify or falsify this explanation, it needs to be checked whether the number of reactants decreases for propagations in a system with an increasing barrier height or not. Figure 4.12 displays the share of reactive particles to the ensemble's total number of particles, over barrier-phases within one oscillation period for different values of the barrier height. Each graph has a minimum at the barrier-phase of $t_0 = 0$ and a maximum roughly around the value of $t_0 = 1.2$ (see Sec. 4.2 for further explanation). For the smallest tested barrier height of $E_\mathrm{b} = 1.0$, the minimum has the largest value out of all the minima-values while it also has the smallest maximum-value out of all the maxima-values. For the largest tested barrier height of $E_\mathrm{b} = 3.0$ this relation is the exact opposite. The movement of a barrier of a high potential energy seems to have a larger impact on the amount of reactions than of a smaller potential energy. However, when averaging over the number of reactions for all barrier-phases, the total numbers of reactions for the barrier heights $E_\mathrm{b} = 1.0$ and $E_\mathrm{b} = 3.0$ are approximately equal with a deviation of only 2%. Hence, altough the particles propagated for a potential with a barrier height of $E_\mathrm{b} = 3.0$ have to overcome a higher potential energy to react, the number of reactions is not reduced. Thus, the hypothesis, that only the fastest particles are able to perform a reaction for large barrier heights is wrong.

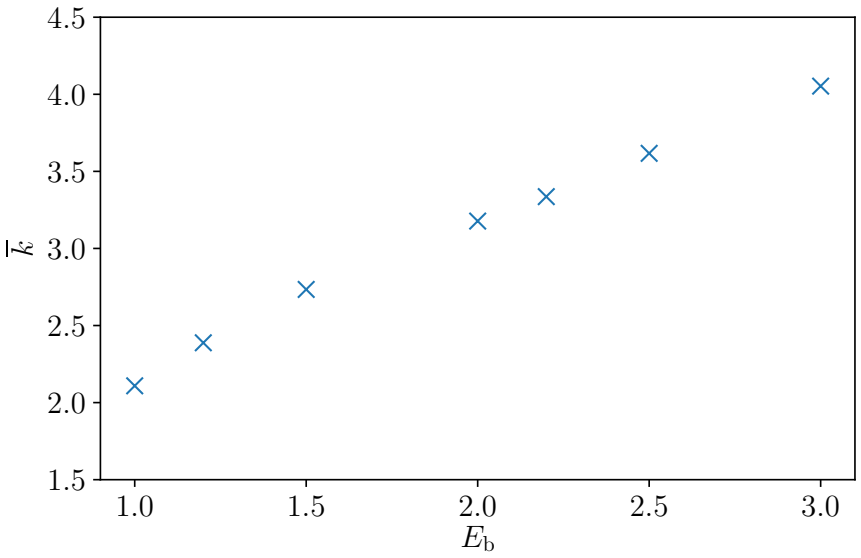

Figure 4.11: Averaged rate $\overline{k}$ vs. the barrier height E_b. The rate increases linearly for increasing values of E_b.

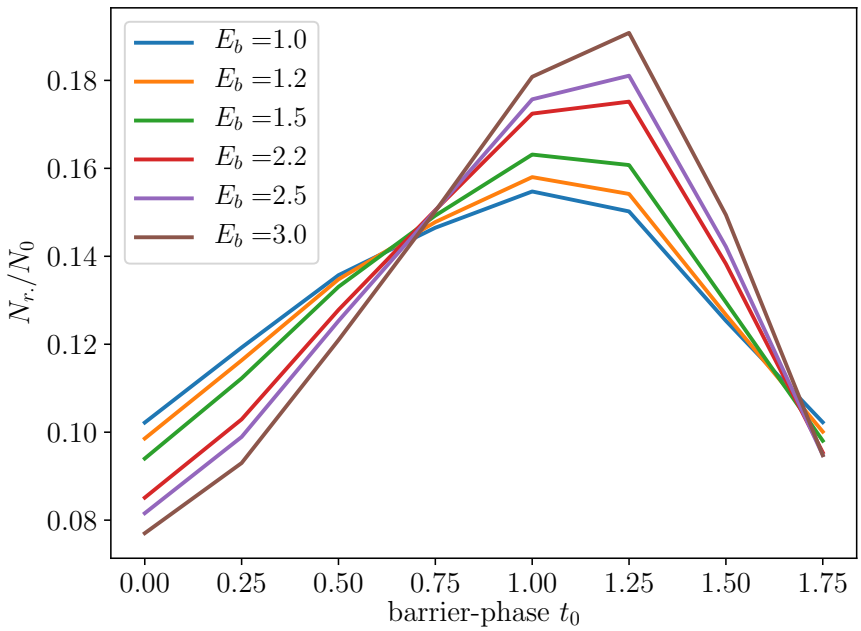

Figure 4.12: Share of reacting particles over the barrier-phase t_0 for several values of E_b.

The number of reactions for different barrier heights can only remain constant if the particles somehow gain at least the same amount of energy they lose while overcoming the barrier. Therefore, it can be assumed that the particles gain more energy when driven by the movements of a system with a higher potential energy than when they are driven by a system with a low potential energy (small barrier height). This gain of energy could result in higher velocities of the particles, which inevitably leads to higher reaction rates.

Fig. 4.13 shows the averaged rate for different values of the barrier's oscillation frequency ω_x. The mean velocity of the barrier is the product of the amplitude and frequency of its oscillation. Hence, the barrier has a higher mean velocity for increasing values of ω_x when the oscillation amplitude $\hat{x}$ remains constant. However, one does not expect to observe a dependence of the rate on the mean velocity of the barrier for the following reason: In Sec. 4.2 it was shown that the rate is partly a reflection of the relative velocity $(v_{\text{Particle}} - v_{\text{Barrier}})$ between the barrier and the particles at the moments of their reaction. When the mean velocity of the barrier increases, the relative velocity is expected to increase whenever the barrier is moving towards the ensemble and to decrease whenever the barrier is moving away from the ensemble. So when averaging over all barrier-phases, these effects are expected to compensate each other and should have no impact on the rate. However, the averaged rates in Fig. 4.13 are not constant for different values of ω_x. The rate is maximized for an oscillation frequency of $\omega_x \approx 4\,\pi/3$ and decreases afterwards. The rate's maximum indicates a kind of "resonance" of the movement of the particles and the barrier for an oscillation frequency of $\omega_x \approx 4\,\pi/3$, leading to an increase of the reaction rate. It is known that the NHIM is in phase with the barrier but has a smaller oscillation amplitude. One could suggest a resonance of the NHIM's amplitude for $\omega_x \approx 4\,\pi/3$ that would lead to a resonance of the rate. However, the NHIM's amplitude shows no such maximum but increases linearly for decreasing values of ω_x. It remains unclear what causes the rate's resonance.

Next, the barrier's oscillation amplitude $\hat{x}$ is varied within a range from 0.0 to 0.8, see Fig. 4.14. Similar to the rates in Fig. 4.13, the averaged rate reaches a maximum and decreases afterwards. The rate is maximized for an oscillation amplitude of $\hat{x} = 0.2$. For an amplitude of $\hat{x} = 0.3$, the value of the respective rate interrupts the monotonous decrease after the maximum was reached. But since the deviation from a monotonous course is below 0.03, it is likely to be due to the general uncertainty of the rate. The barrier's mean velocity also increases linearly with an increasing value of $\hat{x}$. Since the barrier's velocities at the maxima in Figs. 4.14 and 4.13 are not equal, the value of the oscillation amplitude must have an additional impact on the above mentioned resonance of the particles and the barrier.

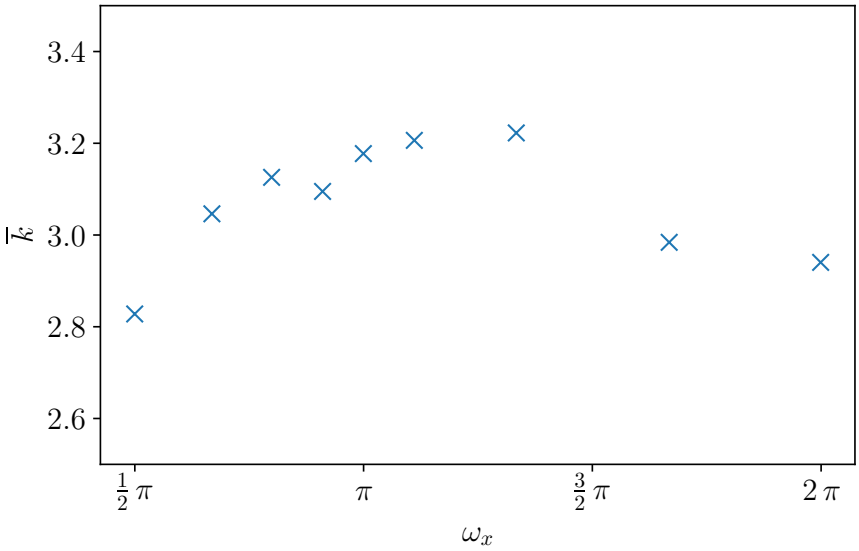

Figure 4.13: Averaged rate $\overline{k}$ vs. the oscillation frequency ω_x of the barrier. The rate reaches a maximum at $\omega_x \approx 4\,\pi/3$.

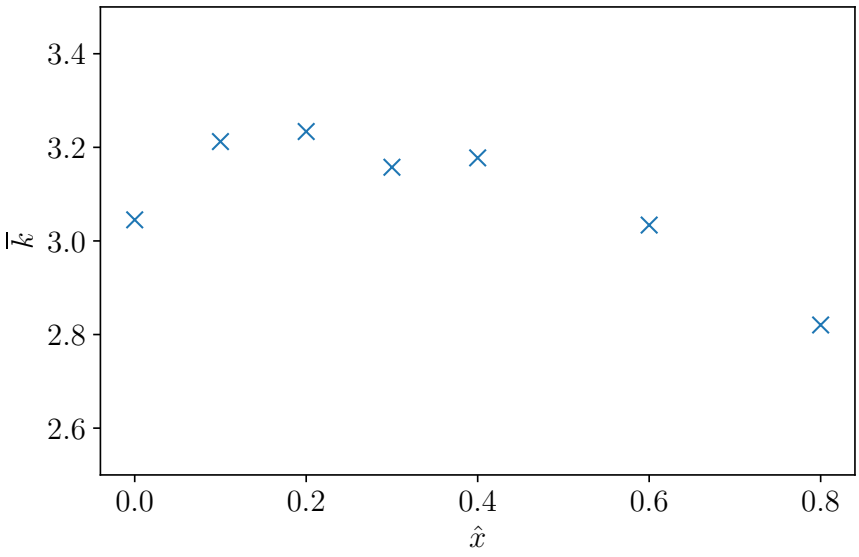

Figure 4.14: Averaged rate $\overline{k}$ vs. the barrier's oscillation amplitude $\hat{x}$. The course of the rate has a maximum at $\hat{x} \approx 0.2$.

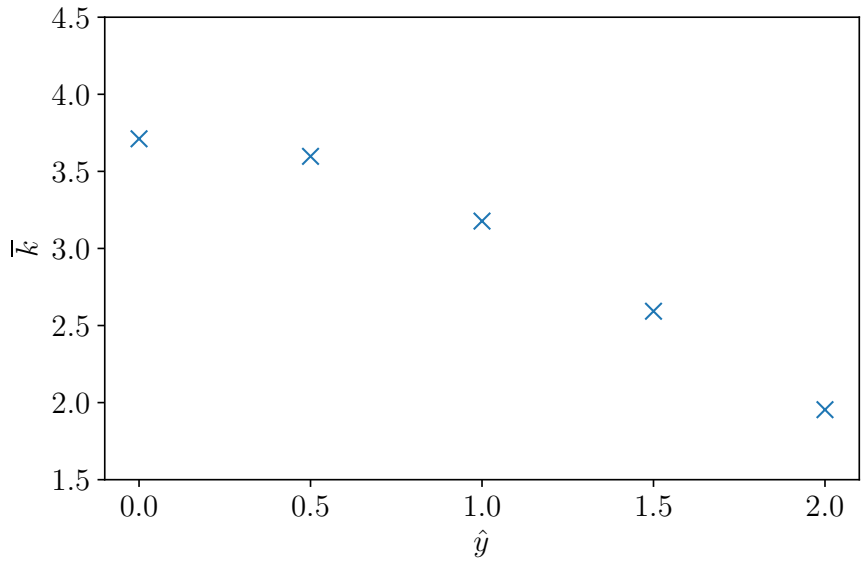

Figure 4.15: Averaged rate $\overline{k}$ vs. the deviation of the potential's minima $\hat{y}$. The rate decreases linearly for increasing values of $\hat{y}$.

Fig. 4.15 shows an approximately linear decrease of the averaged reaction rate for increasing values of the parameter $\hat{y}$ that determines the deviation of the potential's minima from $y = 0.0$. This behavior could be due to increasing length of the saddle in y-direction for an increasing value of $\hat{y}$. When the saddle region is broader, the particles are more likely to be bound to the saddle region for a longer time which may cause their velocities to decrease and therefore lead to a decrease of the reaction rate.

5 Ensemble Positioned Around the NHIM

In Section 4.1.1 it was stated that reactive particles with a small kinetic energy are heavily influenced by the potential's dynamics and therefore have a reaction rate that is a reflection of the potential's properties. When generating an ensemble with a small kinetic energy, the problem of having an insufficient amount of reactive particles arises which leads to bigger fluctuations due to the value of the seed (see Sec. 3.5), for example. This chapter deals with the challenge to find an ensemble that has both, a small kinetic energy and a large amount of reactive particles. Once a new ensemble is introduced, the potential's parameters are again varied and the respective reaction rates are calculated and presented.

5.1 Properties of the Ensemble

Given the ensemble that was propagated in the previous chapter, it was found that only particles with a kinetic energy above a certain value have enough energy to reach the DS and react. This is due to the transformation of kinetic into potential energy while moving up the barrier. When an ensemble has a high potential energy initially, meaning it is positioned closer to the top of the barrier, the particles need less initial kinetic energy to cross the DS. An increase of the potential energy while keeping the kinetic energy constant will indeed increase the number of reactions, but the reacting particles will also have a higher velocity when they do so. Since the goal is to increase the number of slow, yet reacting particles, the ensemble must be positioned closer to the top of the barrier while decreasing the overall kinetic energy. This has to be done in a way that does not inhibit the slowest particles in the ensemble from reacting under advantageous circumstances, such as a barrier moving towards the ensemble. Furthermore, when an ensemble is initialized with a small value of $k_{\mathrm{B}}T$, the distribution of the particle's kinetic energies is more narrow, leading to particles with a more similar and small kinetic energy, which provides a higher concentration of critical particles.

Similar to the ensemble used in the previous chapter, the new ensemble is positioned on the MEP. However, the new ensemble is positioned along the x-axis in a range of

$\Delta x = \pm 0.2$ around the x-position of the dividing surface x_{DS}, which is approximated by its position for the given values of $y = 0$, $v_y = 0$ and the respective phase of the barrier at which the propagation is started. The velocities of the particles are distributed within a restricting range from $v_{x,y} = -10$ to 10. The value of $k_{\mathrm{B}}T$ is chosen to be 0.2. For values smaller than $k_{\mathrm{B}}T = 0.2$ the number of reactants decreases significantly which indicates that particles at the ends of the x-range are no longer able to reach the DS. For each initial barrier-phase, the ensemble has to be generated individually, since the position of the time-dependent DS is different and with it, the x-range changes.

The particles of the ensemble are initialized within the x-range $(x_{\mathrm{DS}} - 0.2,\ x_{\mathrm{DS}} + 0.2)$ as free particles with the potential set to zero to ensure that the kinetic energy distribution is not influenced by the different potential energies within the x-range. They are initialized with positions on the MEP. In order to determine whether a particle crosses the DS, it is necessary to know on which side of the DS it is positioned at the start of the propagation. For each particle, the x-position of the DS is determined through the particle's values of y and v_y. By comparing each particle's x-position to the respective position of the DS, the ensemble is split into two ensembles - one, positioned on the left side of the DS and possibly performing a standard reaction, and another one positioned on the right side of the DS, possibly performing a reverse reaction. The ensemble positioned at x smaller than the x-position of the DS is referred to as the ensemble on the "left" side of the DS, while the other one is refered to as the ensemble on the "right" side of the DS. Ideally, the two ensembles contain the same amount of particles. However, this is not always the case when approximating the position of the whole DS with its position for the values $y = 0.0$ and $v_y = 0.0$. For an initial barrier-phase of $t_0 = 0.5$ the left ensemble contains roughly 33% of all of the initialized particles while the right ensemble contains 67%. For a barrier-phase of $t_0 = 1.5$ these percentages are reversed. This indicates that taking the position of the DS at the values $y = 0.0$ and $v_y = 0.0$ as its average x-position, is just an estimation of its actual position in the x-range of the particles. A possible solution to this issue will be mentioned in the outlook.

Due to the ensemble's low value of $k_{\mathrm{B}}T$, the number of reactive particles is expected to be heavily influenced by the barrier's movement. The share of reactive particles to the total number of particles in each ensemble over the initial phase of the barrier is displayed in Figure 5.1 for both ensembles on the left and right side of the DS. The system is time-dependent and the potential's parameters are set to the standard values. The two ensembles are propagated separately. The graphs show a periodical behavior of N_{r}/N_0, covering one entire period within one period of the barrier's oscillation. The ensemble performing the standard reaction has a maximum share of reactive particles for an initial barrier-phase of $t_0 = 1.0$, whereas the ensemble on the right side of the DS has a minimum share of reacting particles fot this barrier-phase. This is caused by the movement of the barrier at the beginning of its oscillation. For a barrier-phase of $t_0 = 1.0$, the DS moves towards the left ensemble and away from the right ensemble with a maximum velocity. In contrast, the DS moves towards the right ensemble and away

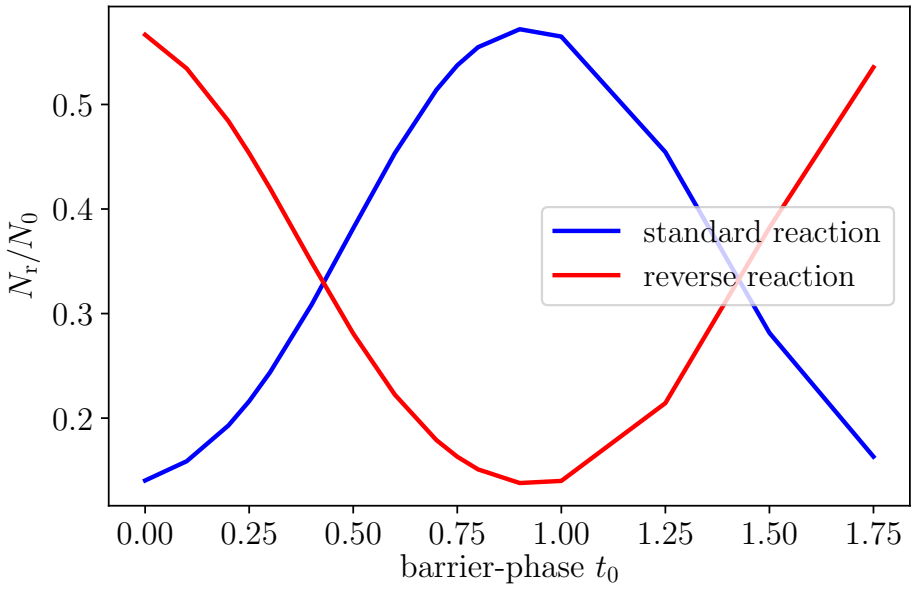

Figure 5.1: Share of reactive particles vs. the phase of the barrier for particles with initial positions left and right of the dividing surface.

from the left ensemble for barrier-phases close to zero, causing a large share of reactive particles in the right ensemble and a small share in the left ensemble. Therefore, the two graphs in Fig. 5.1 are in antiphase. For barrier-phases within one period of the barrier's oscillation, the percentage of reacting particles differs from under 10% up to almost 60% of the total number of particles in the respective ensemble. Considering that only approximately half of the particle's velocities are initialized with a direction towards the barrier, a percentage of almost 60% is a relatively large share of reactive particles. In addition, given the small value of the ensemble's k_BT, these reactive particles are likely to have small kinetic energies and are highly influenced by the system's dynamics. Therefore, the ensemble introduced in this chapter does indeed provide a larger share of slow, yet reactive particles than the previously propagated ensemble, but only for certain values of t_0. In contrast, the high dependence of the low-energy ensemble on the barrier-phase leads to a very low percentage of reacting particles of less than 10% for other values of t_0. When the number of reactants is small, the course of the reactants' population over time is more sensitive to fluctuations and the error due to the fitting-procedure increases. However, whenever one of the two ensembles positioned on the left and right side of the DS contains a small share of reactive particles at a given barrier-phase, the other one inevitably contains a large share of reactive particles. When averaging over the estimated rates of both ensembles, the error due to the fitting-procedure can be slightly compensated.

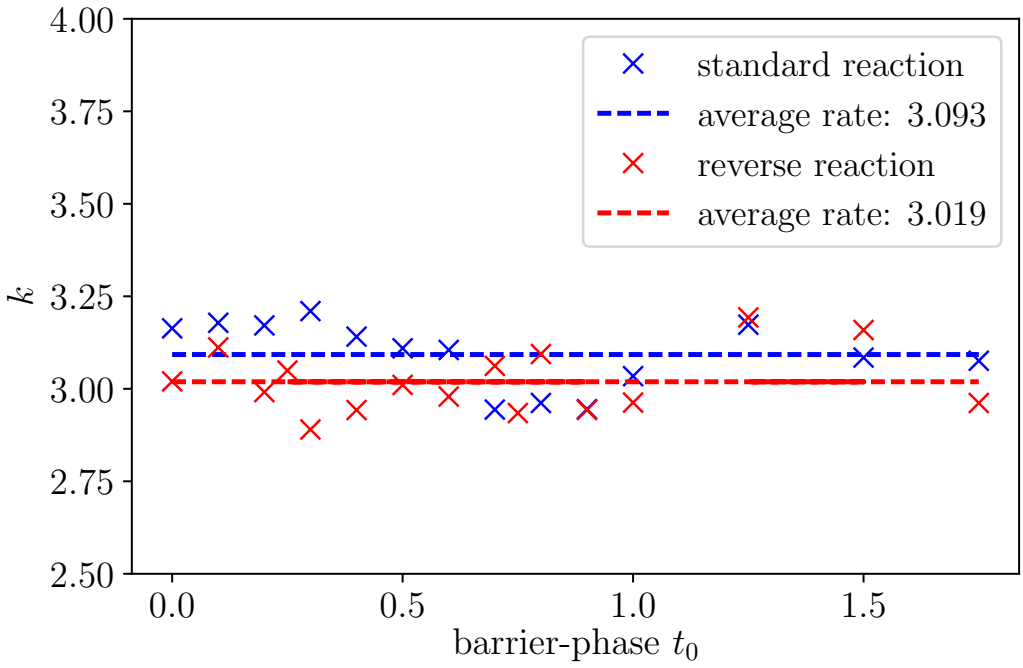

Figure 5.2: Reaction rate vs. the barrier's phase t_0 for an ensemble performing a standard reaction (left ensemble) and one performing a reverse reaction (right ensemble).

Figure 5.2 shows the behavior of the ensembles' rates for different barrier-phases within one period of its oscillation as well as the averaged rates over the phases. The maximum deviation of rates for different t_0 is approximately $\Delta k = 0.3$. Compared to a deviation of up to $\Delta k = 0.7$ of the rates of the ensemble propagated in the previous chapter, this value is relatively low. So although the barrier's phase has a high impact on the number of reactive particles for the ensemble introduced in this chapter, the rate seems to be less affected by this than it was for the ensemble initially positioned further away from the DS. A possible explanation of this behavior is that particles with a small kinetic energy are more likely to be moved along with the barrier rather than maintaining the value and direction of their inital velocity during the reaction. When this happens, the relative velocity of the particles and the barrier remains at a more constant level, leading to a more constant reaction rate.

Another factor that could possibly influence the rate is the change in the potential energies of the particles for different barrier-phases. The position of the DS is not equal to the position of the barrier for barrier-phases other than $t_0 = 0.0$ and $t_0 = 1.0$, because it has a smaller oscillation amplitude than the barrier. For these barrier-phases, the potential is not symmetrical around the DS, like it is around the barrier.

Since the particles are distributed in a fixed range around the DS and not around the barrier, the ensembles have a different distribution of the potential energy for different barrier-phases. However, if a change in the potential energies of the particles lead to a noticable difference in the rates, the courses of the rates of the left compared to the right ensemble in figure 5.2 would be periodic as well as in antiphase to each other. Since this relation can not be observed, it can be assumed that the change in the distribution of the potential energies does not impact the reaction rates significantly. The reaction rate of the ensemble performing a standard reaction shows a similar periodic course as the rates of the ensembles in the last chapter. For the course of the rate of the ensemble that performs the reverse reaction one would expect to observe the reverse periodic behavior. Yet, the course of the rate shows no obvious periodicity. The averaged rates of the two ensembles have a deviation of approximately $\Delta\overline{k} = 0.07$ which is about 2 % of the rates' values and is likely to be due to the general inaccuracy of the fitting-procedure.

5.1.1 The Ensemble's Total Number of Particles

Similar to Sec. 4.3 of the previous chapter, in this section an appropriate number of particles contained by the ensemble is determined. Again, the ensemble should contain the smallest amount of particles possible, while still providing a clear reaction rate whose accuracy and value is close to that of an ensemble containing a large amount of particles. Figure 5.3 shows the averaged rate over the number of particles for two systems with a static and a dynamic potential. The rate is not only averaged over the barrier's phase but it is also the mean value of the rates of the right and left ensemble. Both of the graphs show a convergence for an increasing amount of particles. It is striking that the graph for the static potential converges starting from a reaction rate that is much larger than its final value, whereas the graph of the time dependent potential converges starting from a reaction rate that is only slightly smaller than its final value. Since the rate does not change significantly from $N = 10^6$ to $N = 10^7$, the number of particles contained by the left and right ensemble combined is chosen to be 10^6 for all propagations that are performed in this chapter.

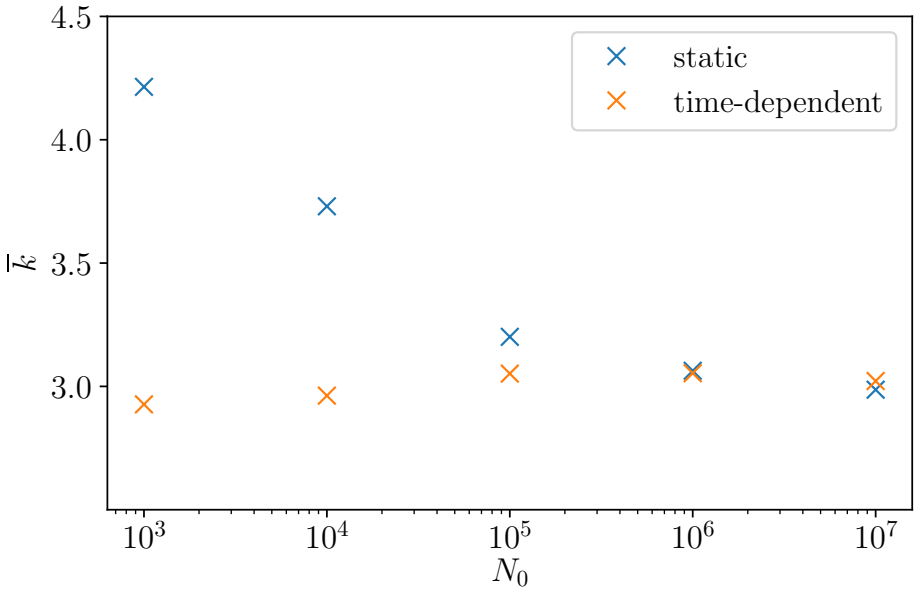

Figure 5.3: Averaged rate vs. the number of particles for a time-dependent and a static potential.

5.2 Modification of the Potential's Parameters

Similar to Sec. 4.4 in the previous chapter, this section deals with the dependence of the reaction rate on the potential's parameters. Again, the parameters E_b, $\hat{x}$, ω_x and $\hat{y}$ are varied. The only difference is in the propagated ensemble. The ensemble used in this section is the one that was introduced at the beginning of this chapter.

Figure 5.4 displays the reaction rate over different values of the barrier height within a range from $E_\mathrm{b} = 1.0$ to $E_\mathrm{b} = 3.0$. The rate is equal to the mean value of the rates of the ensemble on the left and that on the right side of the DS, which are additionally averaged over the barrier-phase. The rate increases linearly from $\overline{k} = 2.2$ up to a value of $\overline{k} = 3.8$. This course is very similar to the course in Fig. 4.11 of the ensemble in Chapt. 4 and is likely to be due to the same cause: particles gain more energy by the movement of systems with a higher potential energy and therefore react faster. However, the share of reactive particles in the ensembles behaves differently for different values of E_b. Figure 5.5 displays the course of the share of reactive particles in the ensemble performing the reverse reaction, over the inital barrier-phases for all of the tested barrier heights. Similar to the system in Chapt. 4, the share of reactive particles has a higher deviation for larger values of E_b. Again, the movement of a barrier of larger height seems to have a bigger impact on the amount of reactions. A difference to the system in Chapt. 4 occurs when summing over all reactions for the different barrier-phases. The

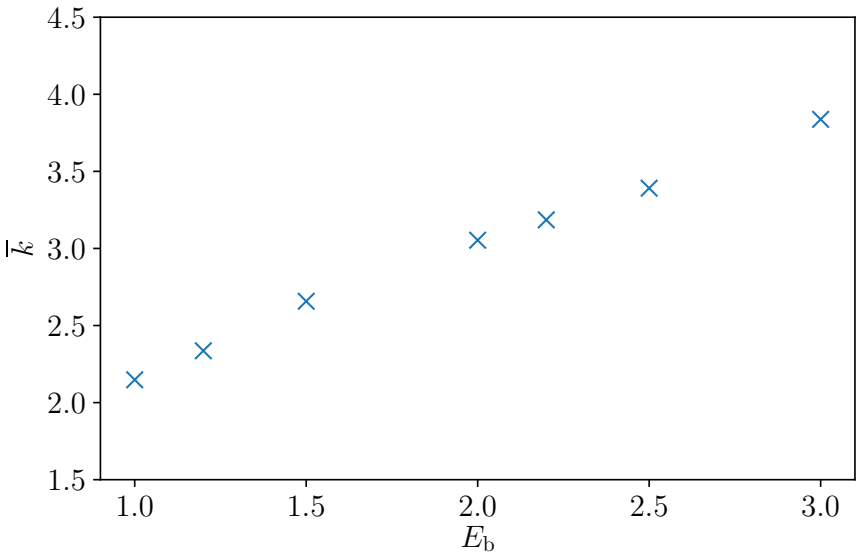

Figure 5.4: Averaged rate $\overline{k}$ vs. the barrier height E_b. The rate increases linearly for increasing values of E_b.

number of reactions is not constant for all barrier heights - it decreases for increasing values of E_b. Since the only difference between the system of this chapter to the system in Chapt. 4 is the ensemble's position and value of $k_\mathrm{B}T$, one of these properties or a combination of the two must be causing the different behavior.

As it was observed in Sec. 5.1, the small value of $k_\mathrm{B}T$ causes the number of reactions to be heavily influenced by the barrier's phase of movement. For increasing values of E_b in Fig. 5.5, the decrease of the number of reactions for barrier-phases for which the barrier is moving away from the ensemble is becoming larger than its increase for barrier phases for which the barrier is moving towards the ensemble. When particles have a low initial potential energy due to their position in the potential energy landscape, while also having a small kinetic energy due to the small value of the ensemble's $k_\mathrm{B}T$, they are less likely to react. Such a particle may perform a reaction when the barrier is moving towards it, but it is almost impossible for it to react when the barrier is additionally moving away from it during the reaction. For an increasing barrier height, there are more particles that have a relatively low potential energy due to the increasing value of the gradient of the potential within the x-range in which the ensemble is initialized. For example, for an initial barrier phase of $t_0 = 0.0$, at which the barrier and the DS are both at $x \approx 0.0$, particles at the edge of the range have a smaller potential energy compared to those positioned close to the top of the barrier. The difference of the particle's potential energies increases with an increasing height of the barrier, leading to more particles with a relatively low potential energy compared to the energy of the barrier they need to

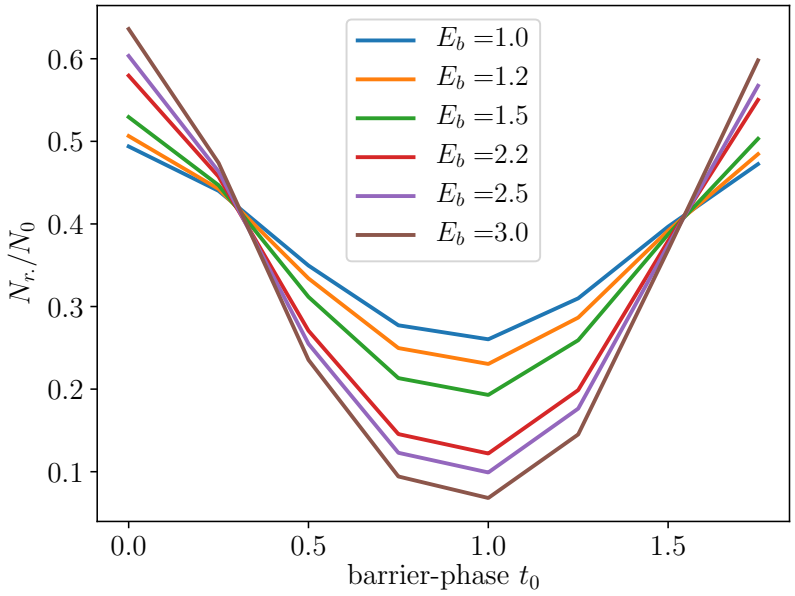

Figure 5.5: Share of reacting particles over the barrier-phase t_0 for all tested values of E_b.

overcome in order to react. This causality could be manifested in the smaller number of reactions for systems with a high barrier.

Another important observation regarding the ensemble's properties for different values of the barrier height is displayed in Fig. 5.6. The plot shows the number of particles contained by the ensemble on the right side of the DS in relation to the total number of particles that are initialized within the whole range around the DS. In a previous section it was already mentioned that choosing the average position of the DS as its position for the values $y = 0$ and $v_y = 0$ is an overestimation for barrier-phases other than $t_0 = 0.0$ and $t_0 = 1.0$. For the barrier-phases 0.5 and 1.5, the DS is deflected the most. This is where the overestimation of the DS's average position is the greatest and leads to a maximum deviation of the share of particles contained by the two ensembles on the left and right side of the DS. The maximum deviation increases for a potential with an increasingly high value of E_b. For a barrier height of 3.0 and $t_0 = 0.5$ the right ensemble contains 70 % of all particles. Ideally, the left and the right ensemble should contain the same share of 50 % of all initialized particles. Therefore, it is necessary to find a solution to the overestimation of the average position of the DS, especially when propagating the ensembles for potentials with a high value of E_b. A possible suggestion on how to overcome this problem will be mentioned in the outlook.

Fig. 5.7 displays the averaged reaction rate for different oscillation frequencies ω_x of

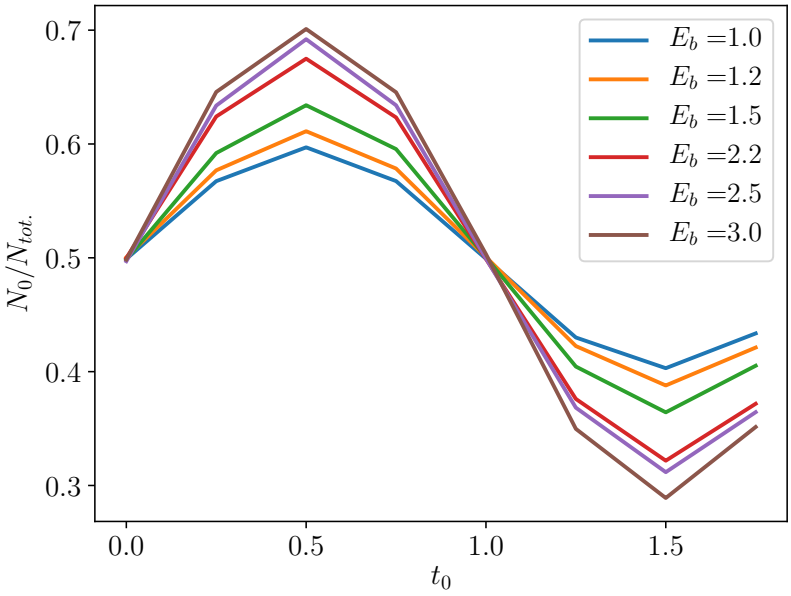

Figure 5.6: Share of particles contained by the ensemble on the right side of the NHIM over the barrier-phase for all tested values of E_b.

the barrier. The rate increases for frequencies up to $\overline{k} = 3.07$, remains constant until $\omega_x = 4\,\pi/3$ and decreases afterwards. Similar to the rate's maximum in Fig. 4.13 in the previous chapter, the high values of $\overline{k}$ are assumed to be due to a resonance effect of the movement of the particles and the barrier.

Fig. 5.7 shows the dependence of the averaged reaction rate on the amplitude $\hat{x}$ of the barrier's oscillation. Unlike in Fig. 4.13 in the previous chapter, the course of the rates does not reach a clear maximum, but remains constant for values from $\hat{x} = 0.0$ to $\hat{x} = 0.4$ and decreases afterwards. Hence, the oscillation amplitude does not seem to impact the reactive behavior of the ensemble that is located in a small range around the DS as much as the one of the ensemble positioned further away from the DS.

Similar to the results in Fig. 4.15 of the previous chapter, Fig. 5.9 shows the same linear decrease of the reaction rate for increasing values of the parameter $\hat{y}$. This behavior is likely to be due to the same reason as for the ensemble of the previous chapter: When the saddle region is broader, the particles are more likely to be bound to the saddle region for a longer time which may cause their velocities to decrease and therefore lead to a decrease of the reaction rate.

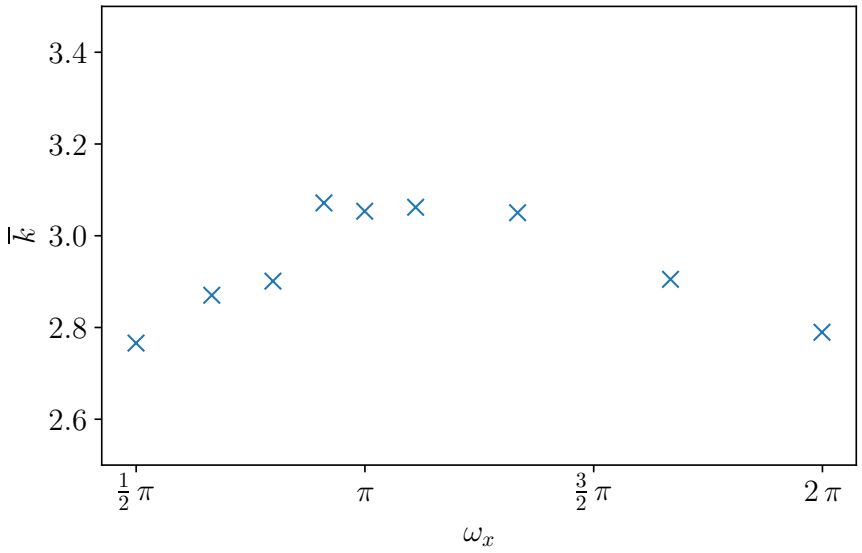

Figure 5.7: Averaged rate $\overline{k}$ vs. the oscillation frequency ω_x of the barrier. The rate reaches its highest value of approximately $\overline{k} = 3.07$ for frequences from $\omega_x = 0.9\,\pi$ to $\omega_x = 4\,\pi/3$ and decreases afterwards.

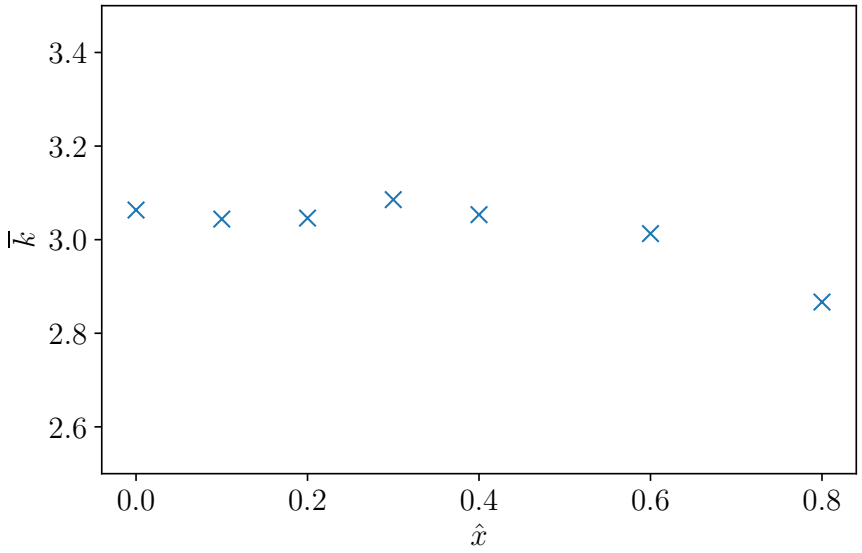

Figure 5.8: Averaged rate $\overline{k}$ vs. the barrier's oscillation amplitude $\hat{x}$. The course of the rate is roughly constant for values from $\hat{x} = 0.0$ to $\hat{x} = 0.4$ and afterwards decreases for increasing values of $\hat{x}$.

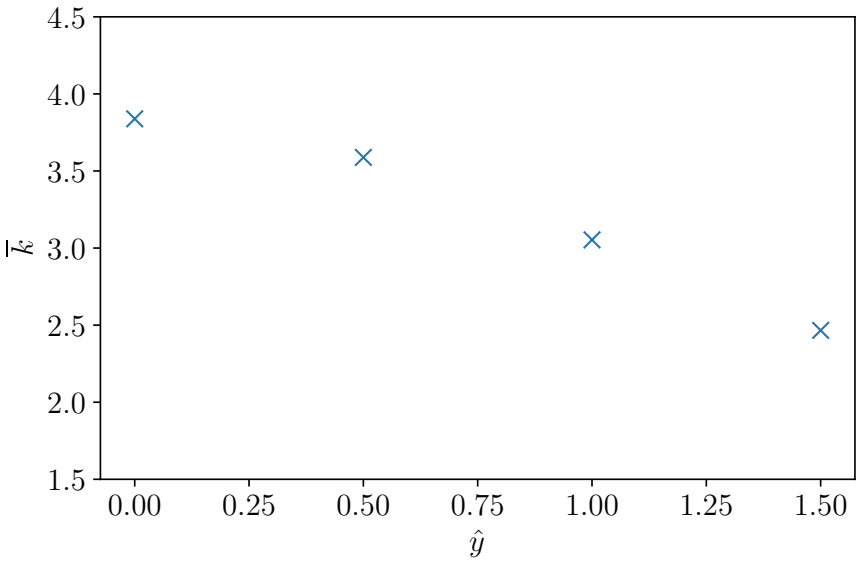

Figure 5.9: Averaged rate $\overline{k}$ vs. the deviation of the potential's minima $\hat{y}$. The rate decreases linearly for increasing values of $\hat{y}$.

6 Conclusion and Outlook

In this work, it was examined if and how several aspects of the simulated system impact the value of the rate constant. It was found that the accuracy of the DS, the chosen fit range for the estimation of the rate constant, the initial phase of movement of the barrier, as well as the ensemble's energy distribution are factors that lead to a deviation of the rate constant. The estimation of the rate constant via a fitting procedure was found to be prone to uncertainties. For future research it might be beneficial to develop a new method of estimating the rates, e.g. by calculating the numerical derivative of the number of reactants over time and determining the rate constant out of it. The impact of the random-number-generator's seed calls for the propagation of more particles which would however increase the computational time of the simulation.

Further, an ensemble with an optimized energy was developed whose reaction rates reflect the system's dynamics rather than depending on the ensemble's properties such as its position on the Minimum-Energy-Path. When propagating this ensemble, the reaction rate showed a periodical dependence on the initial barrier-phase. For different positions of the ensemble on the MEP, this periodical dependence is shifted, while the average reaction rate for various barrier-phases within one period of the barrier's oscillation stays the same. Therefore, the rate constant was usually averaged in order to enable the comparison of rate constants of different systems. By estimating reaction rates for an increasing number of reactants within the ensemble, a total number of $N = 10^6$ was found to be a sufficient amount of particles. The rate constant showed a dependence on all of the potential's parameters that were varied. An increasing barrier height lead to a linear increase of the rate constant. For the variation of the barrier's oscillation frequency as well as for the variation of the amplitude of the oscillation, the rate was maximized for a certain value, respectively. This indicates a resonance between the movement of the barrier and the particles in systems with the respective parameters. For an increasing distance of the potential's minima in y-direction, the rate showed a linear decrease.

Furthermore, the formation of a low-energy ensemble containing a high amount of critical particles was accomplished. It showed a smaller dependence on the initial barrier-phase as the previously propagated ensemble. However, it showed a significantly higher dependence of the number of reactive particles on the barrier-phase. Similar to the previous ensemble, an ensemble containing 10^6 particles was found to be sufficiently suited for the

estimation of the rate constant. The rate constant's dependence on various parameters of the potential was determined. Similar to the course of the rate of the previous ensemble, the rate showed a linear increase for an increasing barrier height. In addition, the approximation of the DS's position that determines the ensemble's position was found to be an overestimation whose inaccuracy increased for an increasing barrier height. A possible solution on how to avoid the issue of approximating the DS's position could be the following: First an equidistant grid of bath coordinates is calculated for which the NHIM's position is then estimated. Afterwards, the particles can be placed on this grid and shifted by a fixed value along the reaction coordinate. Like that, the DS's position does not have to be approximated for the generation of the ensemble. Similar to the rate estimated by propagating the previous ensemble, it reached a maximum for a certain value of the barrier's oscillation frequency, indicating a resonance of the barrier's mean velocity and the movement of the particles. In contrast, the rate remained constant for various oscillation amplitudes. An increasing distance of the potential's minima in y-direction again lead to a linear decrease of the reaction rate.

Throughout this work, it was possible to determine the dependence of the rate constant on many different properties of a two-dimensional time-dependent system. Since the methods used to simulate this system are advanced enough to estimate reaction rates, the next mayor goal would be to simulate a real system, for instance the isomerization of LiCN [37–39]. In the distant future, it might even be possible to predict the impact that a certain external time-dependent field has on a chemical reaction and enable the targeted manipulation of reaction rates in technical applications through external forces.

7 Zusammenfassung in deutscher Sprache

Diese Arbeit befasst sich mit der Bestimmung von Reaktionsraten in einer numerischen Simulation eines zweidimensionalen und zeitabhängigen Systems im Rahmen der Transition State Theory (TST). Insbesondere wird die Reaktionsrate in Abhängigkeit verschiedener Parameter bestimmt, welche die Struktur der Potentiallandschaft des Systems definieren.

In TST kann eine solche Reaktionsrate aus dem Fluss von Reaktanden durch eine Trennfläche berechnet werden, welche den Phasenraum eindeutig in Reaktandenkonfigurationen und Produktkonfigurationen aufteilt. In vergangener Forschungsarbeit am ITP1 konnten mehrere Methoden zur Bestimmung einer zeitabhängigen Hyperfläche entwickelt werden, welche einen mehrdimensionalen und zeitabhängigen Phasenraum eindeutig in die beiden Bereiche trennt. Dies ermöglicht die Berechnung von Reaktionsraten in dieser Arbeit.

Kapitel 2 gibt eine Einführung in die Methoden, welche zur Bestimmung von Reaktionsraten, sowie zur Berechnung der Hyperfläche verwendet werden. Zunächst wird die Bestimmung der Reaktionsrate anhand einer Fit-Funktion, welche den Verlauf der Anzahl an reaktiven Reaktanden über die Zeit annähert, vorgestellt. Zur Berechnung der Hyperfläche wird das Konzept der normal hyperbolischen invarianten Manigfaltigkeit (NHIM) eingeführt, welche die Position der Hyperfläche auf der Reaktionskoordinate definiert. Zudem wird auf die Bestimmung einer zeitlich und räumlich kontinuierlichen Hyperfläche mittels der Interpolation vieler Datenpunkte durch ein Neuronales Netz eingegangen. In Kapitel 2 findet sich außerdem eine kurze Vorstellung des, für die Simulationen in dieser Arbeit verwendeten, Systems, einschließlich der Struktur des zeitabhängigen zweidimensionalen Rang-1 Sattelpotentials, der Art des propagierten Ensembles, dem Aufbau des verwendeten Neuronalen Netzes, sowie die auf das System angepasste Ratenbestimmung.

Kapitel 3 legt dar, wie verschiedene Aspekte des Systems den Wert der Reaktionsrate, teilweise in ungewünschter Weise, beeinflussen. Dazu wird zunächst auf den Einfluss von mehrfach reagierenden Teilchen eingegangen, deren Existenz die Bestimmung der Rate erschweren. Der Abschnitt zeigt, wie wichtig es ist, ein Neuronales Netz zu entwickeln,

welches eine Hyperfläche mit großer Genauigkeit annähert. Das, in dieser Arbeit verwendete, Netz zeichnet sich durch die Representation einer Hyperfläche mit einer sehr kleinen Anzahl an mehrfach reagierenden Teilchen aus. Auch die Wahl des Fit-Bereichs hat einen großen Einfluss auf den Wert der Reaktionsrate. Für höherenergetische Ensemble hängt die Rate verstärkt vom Fit-Bereich ab. Dieser Abschnitt macht deutlich, dass es sinnvoll ist, für die Simulationen stets Ensemble derselben Energie, sowie einen ähnlichen Fit-Bereich für die Ratenbestimmung zu wählen. Auch die Phase der Oszillation der zeitabhängigen Potentialbarriere beeinflusst die Rate. Um verschiedene Systeme miteinander vergleichen zu können, wird die Rate für gewöhnlich über 8 verschiedene Phasen innerhalb einer Periode gemittelt. Es wird außerdem aufgezeigt, dass es für ein statisches Potential zu einer Unsicherheit der Rate für verschiedenen Barrierenphasen kommt, welche allerdings leicht vermieden werden kann, wenn man die Hyperfläche in diesem Fall zeitunabhängig interpoliert. Zuletzt wird in Kapitel 3 noch auf den Einfluss des sogenannten „seeds“ des Zufallsgenerators auf die Rate eingegangen, welcher zur Generierung des Ensembles verwendet wird. Um diese Abhängigkeit zu vermeiden sollte eine größere Anzahl von Teilchen propagiert werden, was aufgrund des höheren Zeitaufwands in dieser Arbeit allerdings nicht umgesetzt werden konnte.

Kapitel 4 beschäftigt sich mit der Ratenrechnung mit einem geeigneten Ensemble. Zunächst wird beobachtet, dass die Rate eines Ensembles, welches in y-Richtung ausgedehnt ist, eine exponentielle Abhängigkeit von der Position des Ensembles entlang der Reaktionskoordinate x aufzeigt. Durch einige Untersuchungen wird ein neues Ensemble ermittelt, welches auf einem Punkt auf dem Pfad der minimalen Energie im Potential platziert ist und für welches die Abhängigkeit der Rate von der Position des Ensembles verschwindet. Anschließend wird die Energie des Ensembles optimiert. Es zeigt sich, dass die Rate von Ensemblen mit sehr hoher Energie unbeeinflusst von der Bewegung der Potentialbarriere ist, was nicht dem Zweck dient, Reaktionsraten in Abhängigkeit zeitlich getriebener Systeme zu bestimmen. Ist die Energie des Ensembles zu klein, reagieren signifikant weniger Teilchen, was wiederum die Ratenbestimmung erschwert. Schließlich wird eine Energie gewählt, bei welcher ausreichend viele Teilchen reagieren, sowie die Rate von der Bewegung des Potentials abhängt. Anschließend wird eine periodische Abhängigkeit der Rate, sowie der Anzahl an Reaktionen von der Barrierenphase festgestellt und Theorien zu deren Ursachen aufgestellt. Eine Bewegung der Barriere entgegen der Bewegung der Teilchen scheint zu einer hohen Reaktionsrate zu führen, während eine Bewegung in entgegengesetzter Richtung zu einer kleinen Reaktionsrate führt. Um die optimale Anzahl an Teilchen in einem Ensemble zu bestimmen, wird die Reaktionsrate für verschiedene Teilchenzahlen bestimmt. Es zeigt sich eine Konvergenz der Rate gegen einen festen Wert für größer werdende Teilchenzahlen. Ab einer Teilchenzahl von 10^6 stimmt die Rate ausreichend genau mit diesem Wert überein, weshalb die Teilchenzahl des Ensembles für alle Propagationen zu 10^6 gewählt wird. Zuletzt werden verschiedene Parameter des Potentials variiert und die jeweilige Reaktionsrate bestimmt. Die Rate zeigt einen linearen Anstieg für eine höher werdende Potentialbarriere. Für die Varia-

tion der Oszillationsfrequenz der Barriere zeigte sich eine Resonanz der Rate für eine bestimmte Frequenz. Selbiges zeigte sich bei der Variation der Oszillationsamplitude. Auf die genauen Ursachen dieses Resonanzeffekts konnte nicht geschlossen werden. Für einen größer werdenden Abstand der beiden Täler des Potentials zeigte die Rate einen linearen Abfall.

Das Ziel von Kapitel 5 ist die Erhöhung der Anzahl an sogenannten kritischen Teilchen im Ensemble. Die Reaktionsrate dieser Teilchen gibt besonders viel Aufschluss über die Dynamik des Potentials, da sie lange in der Sattelregion verweilen. Dazu wird ein niederenergetisches Ensemble in einem kleinen Bereich auf dem MEP entlang der Reaktionskoordinate um die Position der trennenden Hyperfläche herum positioniert. Das Ensemble wird in ein Ensemble links und rechts von der Hyperfläche getrennt und die sich ergebenden Ensembles werden seperat propagiert. Es wird eine kleinere Abhängigkeit der Reaktionsrate dieser Ensemble von der Barrierenphase festgestellt. Jedoch zeigt die Anzahl an Reaktionen, aufgrund der niederen kinetischen Energie der Ensemble, eine ausgesprochen hohe Abhängigkeit von der Barrierenphase. Wie für das Ensemble in Kapitel 4, zeigt sich eine Anzahl von 10^6 Teilchen auch für dieses Ensemble als ausreichend. Zuletzt wird auch für Propagationen mit dem neuen Ensemble die Abhängigkeit der Rate für verschiedene Potentialparameter untersucht. Die Abhängigkeit der Reaktionsrate von der Barrierenhöhe, der Oszillationsfrequenz, sowie des Abstands der Täler im Potential ist, bis auf kleine Abweichungen, äquivalent zu der Abhängigkeit, welche in Kapitel 4 beobachtet wurde. Für die Variation der Oszillationsfrequenz zeigt die Rate allerdings eine deutlich schwächere Abhängigkeit als die Rate für das Ensemble in Kapitel 4.

Für zukünftige Untersuchungen in diesem Bereich wäre es interessant, die Bestimmung von Raten in einem realen System zu ermöglichen. Ein solches System wäre zum Beispiel die Isomerisation von LiCN. In ferner Zukunft könnte die numerische Ratenberechnung in getriebenen Systemen Vorhersagungen für reale technische Anwendungen treffen und die gezielte Beeinflussung des Reaktionsverhalten chemischer Stoffe ermöglichen.

Bibliography

1. Pitzer, K. S., Smith, F. T. & Eyring, H. *The Transition State* 53 (Chemical Society, London, 1962).
2. Pechukas, P. Transition State Theory. *Annu. Rev. Phys. Chem.* **32,** 159–177 (1981).
3. B. C. Garrett & D. G. Truhlar. Generalized Transition State Theory. *J. Phys. Chem.* **83,** 1052–1079 (1979).
4. D. G. Truhlar, A. D. Issacson & B. C. Garrett. in (ed M. Baer) 65–137 (CRC Press, Boca Raton, FL, 1985).
5. Hynes, J. T. Chemical reaction dynamics in solution. *Annu. Rev. Phys. Chem.* **36,** 573–597 (1985).
6. Berne, B. J., Borkovec, M. & Straub, J. E. Classical and modern methods in reaction rate theory. *J. Phys. Chem.* **92,** 3711–3725 (1988).
7. Nitzan, A. Activated rate processes in condensed phases: The Kramers theory revisited. *Adv. Chem. Phys.* **70,** 489–555 (1988).
8. Hänggi, P., Talkner, P. & Borkovec, M. Reaction-rate theory: Fifty years after Kramers. *Rev. Mod. Phys.* **62.** and references therein, 251–341 (1990).
9. Natanson, G. A., Garrett, B. C., Truong, T. N., Joseph, T. & Truhlar, D. G. The Definition of Reaction Coordinates for Reaction-Path Dynamics. *J. Chem. Phys.* **94,** 7875–7892 (1991).
10. Truhlar, D. G., Garrett, B. C. & Klippenstein, S. J. Current Status of Transition-State Theory. *J. Phys. Chem.* **100,** 12771–12800 (1996).
11. Truhlar, D. G. & Garrett, B. C. Multidimensional Transition State Theory and the Validity of Grote-Hynes Theory. *J. Phys. Chem. B* **104,** 1069–1072 (2000).
12. Komatsuzaki, T. & Berry, R. S. Dynamical hierarchy in transition states: Why and how does a system climb over the mountain? *Proc. Natl. Acad. Sci. U.S.A.* **98,** 7666–7671 (2001).
13. Pollak, E. & Talkner, P. Reaction rate theory: What it was, where it is today, and where is it going? *Chaos* **15,** 026116 (2005).
14. Waalkens, H., Schubert, R. & Wiggins, S. Wigner's dynamical transition state theory in phase space: classical and quantum. *Nonlinearity* **21,** R1 (2008).

15. Bartsch, T., Moix, J. M., Hernandez, R., Kawai, S. & Uzer, T. Time-dependent transition state theory. *Adv. Chem. Phys.* **140,** 191–238 (2008).

16. Kawai, S. & Komatsuzaki, T. Robust Existence of a Reaction Boundary to Separate the Fate of a Chemical Reaction. *Phys. Rev. Lett.* **105,** 048304 (4 2010).

17. Hernandez, R., Bartsch, T. & Uzer, T. Transition State Theory in Liquids Beyond Planar Dividing Surfaces. *Chem. Phys.* **370,** 270–276 (2010).

18. Sharia, O. & Henkelman, G. Analytic dynamical corrections to transition state theory. *New J. Phys.* **18,** 013023 (2016).

19. Feldmaier, M., Junginger, A., Main, J., Wunner, G. & Hernandez, R. Obtaining time-dependent multi-dimensional dividing surfaces using Lagrangian descriptors. *Chem. Phys. Lett.* **687,** 194 (2017).

20. Schraft, P., Junginger, A., *et al.* Neural network approach to time-dependent dividing surfaces in classical reaction dynamics. *Phys. Rev. E* **97,** 042309 (2018).

21. Bardakcioglu, R., Junginger, A., Feldmaier, M., Main, J. & Hernandez, R. Binary contraction method for the construction of time-dependent dividing surfaces in driven chemical reactions. *Phys. Rev. E* **98,** 032204 (2018).

22. Bardakcioglu, R. Time-Dependent Transition State Theory to Determine Dividing Surfaces and Reaction Rates in Multidimensional Systems. *Master's Thesis (2018).*

23. Lichtenberg, A. J. & Liebermann, M. A. *Regular and Stochastic Motion* (Springer, New York, 1982).

24. Ott, E. *Chaos in dynamical systems* Second edition (Cambridge University Press, Cambridge, 2002).

25. Wiggins, S. *Normally hyperbolic invariant manifolds in dynamical systems* (Springer Science & Business Media, 2013).

26. Bartsch, T., Hernandez, R. & Uzer, T. Transition state in a noisy environment. *Phys. Rev. Lett.* **95,** 058301 (2005).

27. Bartsch, T., Uzer, T. & Hernandez, R. Stochastic transition states: Reaction geometry amidst noise. *J. Chem. Phys.* **123,** 204102 (2005).

28. Bartsch, T., Uzer, T., Moix, J. M. & Hernandez, R. Identifying Reactive Trajectories Using a Moving Transition State. *J. Chem. Phys.* **124,** 244310 (2006).

29. Kawai, S. & Komatsuzaki, T. Dynamic pathways to mediate reactions buried in thermal fluctuations. I. Time-dependent normal form theory for multidimensional Langevin equation. *J. Chem. Phys.* **131,** 224505 (2009).

30. Craven, G. T., Bartsch, T. & Hernandez, R. Persistence of transition state structure in chemical reactions driven by fields oscillating in time. *Phys. Rev. E* **89,** 040801(R) (2014).

31. Craven, G. T., Bartsch, T. & Hernandez, R. Communication: Transition State Trajectory Stability Determines Barrier Crossing Rates in Chemical Reactions Induced by Time-Dependent Oscillating Fields. *J. Chem. Phys.* **141,** 041106 (2014).

32. Craven, G. T., Bartsch, T. & Hernandez, R. Chemical reactions induced by oscillating external fields in weak thermal environments. *J. Chem. Phys.* **142,** 074108 (2015).

33. Junginger, A. & Hernandez, R. Uncovering the geometry of barrierless reactions using Lagrangian descriptors. *J. Phys. Chem. B* **120,** 1720 (2016).

34. Junginger, A., Craven, G. T., *et al.* Transition state geometry of driven chemical reactions on time-dependent double-well potentials. *Phys. Chem. Chem. Phys.* **18,** 30270 (2016).

35. Junginger, A. & Hernandez, R. Lagrangian descriptors in dissipative systems. *Phys. Chem. Chem. Phys.* **18,** 30282 (2016).

36. Junginger, A., Duvenbeck, L., *et al.* Chemical dynamics between wells across a time-dependent barrier: Self-similarity in the Lagrangian descriptor and reactive basins. *J. Chem. Phys.* **147,** 06401 (2017).

37. Garcia-Müller, P. L., Hernandez, R., Benito, R. M. & Borondo, F. The role of the CN vibration in the activated dynamics of LiNC LiCN isomerization in an argon solvent at high temperatures. *J. Chem. Phys.* **141,** 074312 (2014).

38. Junginger, A., Garcia-Muller, P. L., Borondo, F., Benito, R. M. & Hernandez, R. Solvated molecular dynamics of LiCN isomerization: All-atom argon solvent versus a generalized Langevin bath. *J. Chem. Phys.* **144,** 024104 (2016).

39. García-Müller, P. L., Hernandez, R., Benito, R. M. & Borondo, F. Detailed study of the direct numerical observation of the Kramers turnover in the LiNC=LiCN isomerization rate. *J. Chem. Phys.* **137,** 204301 (2012).

40. Ulusoy, I. S., Stanton, J. F. & Hernandez, R. Effects of roaming trajectories on the transition state theory rates of a reduced-dimensional model of ketene isomerization. *J. Phys. Chem. A* **117,** 7553–7560 (2013).

41. Ulusoy, I. S., Stanton, J. F. & Hernandez, R. Correction to 'Effects of roaming trajectories on the transition state theory rates of a reduced-dimensional model of ketene isomerization'. *J. Phys. Chem. A* **117,** 10567 (2013).

42. Ulusoy, I. S. & Hernandez, R. Revisiting roaming trajectories in ketene isomerization at higher dimensionality. *Theor. Chem. Acc.* **133,** 1528. ISSN: 1432-881X (2014).

43. Craven, G. T. & Hernandez, R. Deconstructing field-induced ketene isomerization through Lagrangian descriptors. *Phys. Chem. Chem. Phys.* **18,** 4008–4018 (2016).

44. Mendoza, C. & Mancho, A. M. Hidden Geometry of Ocean Flows. *Phys. Rev. Lett.* **105,** 038501 (3 2010).

45. Mancho, A. M., Wiggins, S., Curbelo, J. & Mendoza, C. Lagrangian Descriptors: A Method for Revealing Phase Space Structures of General Time Dependent Dynamical Systems. *Commun. Nonlinear Sci. Numer. Simul.* **18,** 3530–3557 (2013).

46. Craven, G. T. & Hernandez, R. Lagrangian descriptors of thermalized transition states on time-varying energy surfaces. *Phys. Rev. Lett.* **115,** 148301 (2015).

47. Schraft, P. Neural networks for the approximation of time-dependent dividing surfaces in Trasition State Theory. *Master's Thesis (2017).*

Danksagung

Zuletzt möchte ich mich bei allen bedanken, die mich beim Schreiben meiner Bachelorarbeit unterstützt haben. Mein Dank gilt insbesondere

- Apl. Prof. Dr. Jörg Main für die Möglichkeit meine Bachelorarbeit über dieses spannende Thema am ITP1 zu schreiben.
- Matthias Feldmaier für die ausgesprochen gute Betreuung und gelegentliche seelische Unterstützung.
- Allen weiteren Mitgliedern der TST-Forschungsgruppe am ITP1, die mich in ihre interessanten Diskussionen miteinbezogen haben und mir stets mit Rat und Tat zur Seite standen: Johannes Reiff, Martin Tschöpe, Philippe Schraft, Robin Bardakcioglu und Tobias Mielich.
- Allen Besuchern der legendären und einzigartigen Kaffeerunde am ITP1, welche sehr oft das Highlight meines Tages darstellte und mein Weltbild in alle nur erdenklichen Richtungen erweiterte.
- Meiner tollen Lerngruppe, ohne die der Bachelor nur halb so schön gewesen wäre.
- Meiner Schwester Jessica Lober, ohne die diese Bachelorarbeit keine Kommas enthalten würde.
- Meinem kleinen grünen Kaktus, welcher mir beim Schreiben der Bachelorarbeit stets Gesellschaft leistete.
- Mandelmus, für die perfekte Vereinigung von Geschmack und Cremigkeit.

Ehrenwörtliche Erklärung

Ich erkläre,

- dass ich diese Bachelorarbeit selbständig verfasst habe,
- dass ich keine anderen als die angegebenen Quellen benutzt und alle wörtlich oder sinngemäß aus anderen Werken übernommenen Aussagen als solche gekennzeichnet habe,
- dass die eingereichte Arbeit weder vollständig noch in wesentlichen Teilen Gegenstand eines anderen Prüfungsverfahrens gewesen ist,
- dass ich die Arbeit weder vollständig noch in Teilen bereits veröffentlicht habe, es sei denn, der Prüfungsausschuss hat die Veröffentlichung vorher genehmigt
- und dass das elektronische Exemplar mit den anderen Exemplaren übereinstimmt.

Stuttgart, den 26. August, 2018 *Melissa Jacqueline Lober*